*Ann. Rev. Astron. Astrophys. 1984. 22 : 319–58*


# EXTRAGALACTIC RADIO JETS

*Alan H. Bridle*

National Radio Astronomy Observatory,[1] Charlottesville, Virginia 22901

*Richard A. Perley*

National Radio Astronomy Observatory, Socorro, New Mexico 87801

## 1. INTRODUCTION

Powerful extended extragalactic radio sources pose two vexing astrophysical problems [reviewed in (147) and (157)]. First, from what energy reservoir do they draw their large radio luminosities (as much as $10^{38}$ W between 10 MHz and 100 GHz)? Second, how does the active center in the parent galaxy or QSO supply as much as $10^{54}$ J in relativistic particles and fields to radio "lobes" up to several hundred kiloparsecs outside the optical object? New aperture synthesis arrays (68, 250) and new image-processing algorithms (66, 101, 202, 231) have recently allowed radio imaging at subarcsecond resolution with high sensitivity and high dynamic range; as a result, the complexity of the brighter sources has been revealed clearly for the first time. Many contain *radio jets*, i.e. narrow radio features between compact central "cores" and more extended "lobe" emission. This review examines the systematic properties of such jets and the clues they give to the physics of energy transfer in extragalactic sources. We do not directly consider the jet production mechanism, which is intimately related to the first problem noted above—for reviews, see (207) and (251).

### 1.1 *Why "Jets"?*

Baade & Minkowski (3) first used the term *jet* in an extragalactic context, describing the train of optical knots extending $\sim 20''$ from the nucleus of M87; the knots resemble a fluid jet breaking into droplets. They suggested

[1] The National Radio Astronomy Observatory is operated by Associated Universities, Inc. under contract with the National Science Foundation.



0066–4146/84/0915–0319$02.00

that "the jet was formed by ejection from the nucleus" (even though its continuous spectrum gave no clue to its velocity) and that an [OII] $\lambda$3727 emission line in the nucleus whose centroid is blueshifted by several hundred kilometers per second from the systemic velocity is "emitted by a part of the material which forms the jet and is still very close to, if not still inside, the nucleus." The "optical wisp" (227) near the QSR 3C 273, which resembles the M87 knots, was also called a *jet* without direct evidence for outflow. Radio detection of these optical "jets" (114, 160) prompted description of narrow features in other 3C sources (168, 253) as "radio jets." In 1973, refined versions of the continuous outflow, or "beam," models for extragalactic sources proposed earlier by Morrison (162) and Rees (204) were developed (25, 147, 221). The new models (*a*) obviated adiabatic losses, which led "explosive" models to require that the compact precursors of extended sources be far more luminous than any actually observed; and (*b*) they explained how the synchrotron lifetimes of electrons in bright lobe "hot spots" can be less than the light travel time to the hot spots from the parent galaxy or QSR (e.g. 113). Continuous flow models and jet data have kept close company ever since.

1.1.1 CAVEAT The term *jet* connotes continuous outflow of fluid from a collimator, but there is no direct evidence for flow in any continuous extragalactic "jet." VLBI studies of proper motions of knots in some compact radio sources—reviewed in (57)—suggest outflow of jetlike features from stationary "cores," but only in 3C 345 (7) has this been tested in an external reference frame. Such proper motions cannot be monitored in truly continuous emission. Narrow kiloparsec-scale features are therefore called *jets* mainly because they occur where "beam" models required collimated outflow from active nuclei.

## 1.2 *What Makes a "Narrow Feature" a "Jet"?*

Terminology that so prejudges source physics should be used sparingly, so we require (as in 27) that to be termed a *jet*, a feature must be

1. at least four times as long as it is wide,
2. separable at high resolution from other extended structures (if any), either by brightness contrast or spatially (e.g. it should be a narrow ridge running through more diffuse emission, or a narrow feature in the inner part of a source entering more extended emission in the outer part),
3. aligned with the compact radio core where it is closest to it.

1.2.1 EXAMPLES Figures 1 to 5 show examples of jets of various powers and sizes. They also illustrate some ambiguities—with less sensitivity, the NGC 6251 jet (Figure 2) breaks into discrete knots, not all of which are

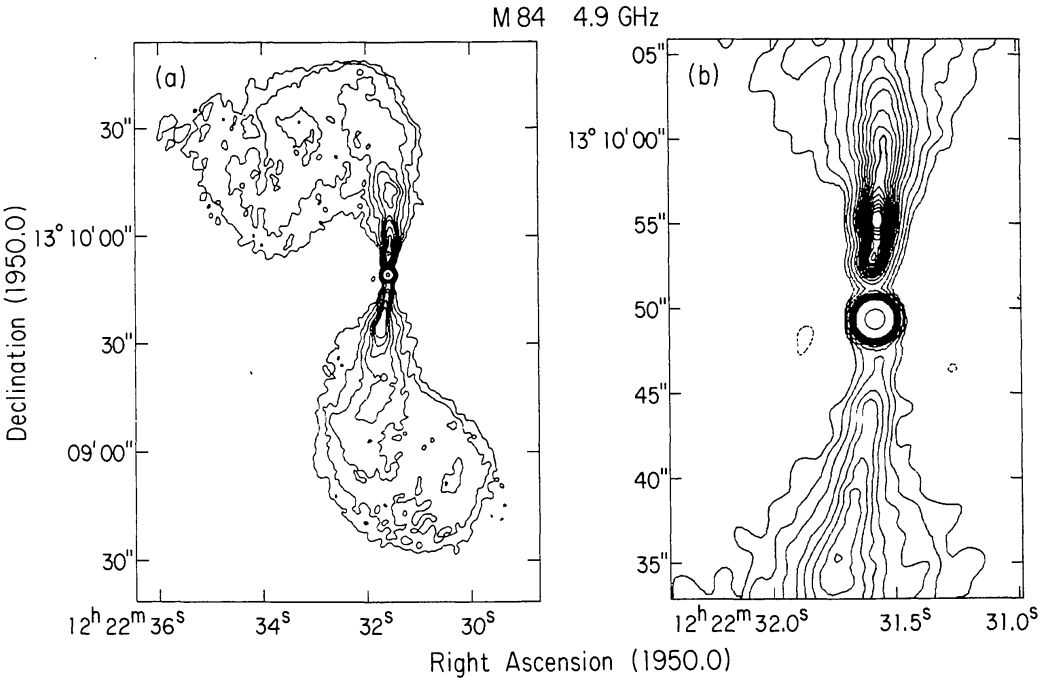


*Figure 1* VLA maps of the jets in the weak radio galaxy M84 at 4.9 GHz, with the right panel showing detail of the central region. The peak on these maps is the radio core. Note the one-sided bright base of the northern jet and the faint cocoon of emission flaring from both jets beyond 5″ from the core (data of R. A. Laing and A. H. Bridle, in preparation).

elongated along it. We call a train of knots a *jet*, however, only if it has more than two knots or if some knots are elongated along it (e.g. Figures 3 and 5). (We prefer to exclude some blobby jets temporarily than to apply the prejudicial term *jet* too liberally.) The elongated outer lobes of some edge-darkened sources, e.g. 3C 31 (245), may equally plausibly be termed broad jets (87), so dividing them into "jet" and "lobe" segments by morphology alone may be subjective. We ask that they contain a "spine" of bright emission meeting criterion (2.) before we call them *jets*.

## 2. THE INCIDENCE OF EXTRAGALACTIC RADIO JETS

### 2.1 *A List of Known Jets*

Table 1 lists data on 125 radio sources known to us (in mid-August 1983) to have *jets* by our criteria. (We use $H_0 = 100$ km s$^{-1}$ Mpc$^{-1}$ and $q_0 = 0.5$.) Column 2 gives the identification—galaxy (G) or quasar (Q)—and its redshift. Columns 3 and 4 measure the observer's frame core and total monochromatic powers—$\log_{10} P^5_{\rm core}$ at 5 GHz and $\log_{10} P^{1.4}_{\rm tot}$ at 1.4 GHz. (The flux densities $S^5_{\rm core}$ and $S^{1.4}_{\rm tot}$ are those most often available.) We use "typical" values for variable cores. Some $S^5_{\rm core}$ and $S^{1.4}_{\rm tot}$ values are estimated

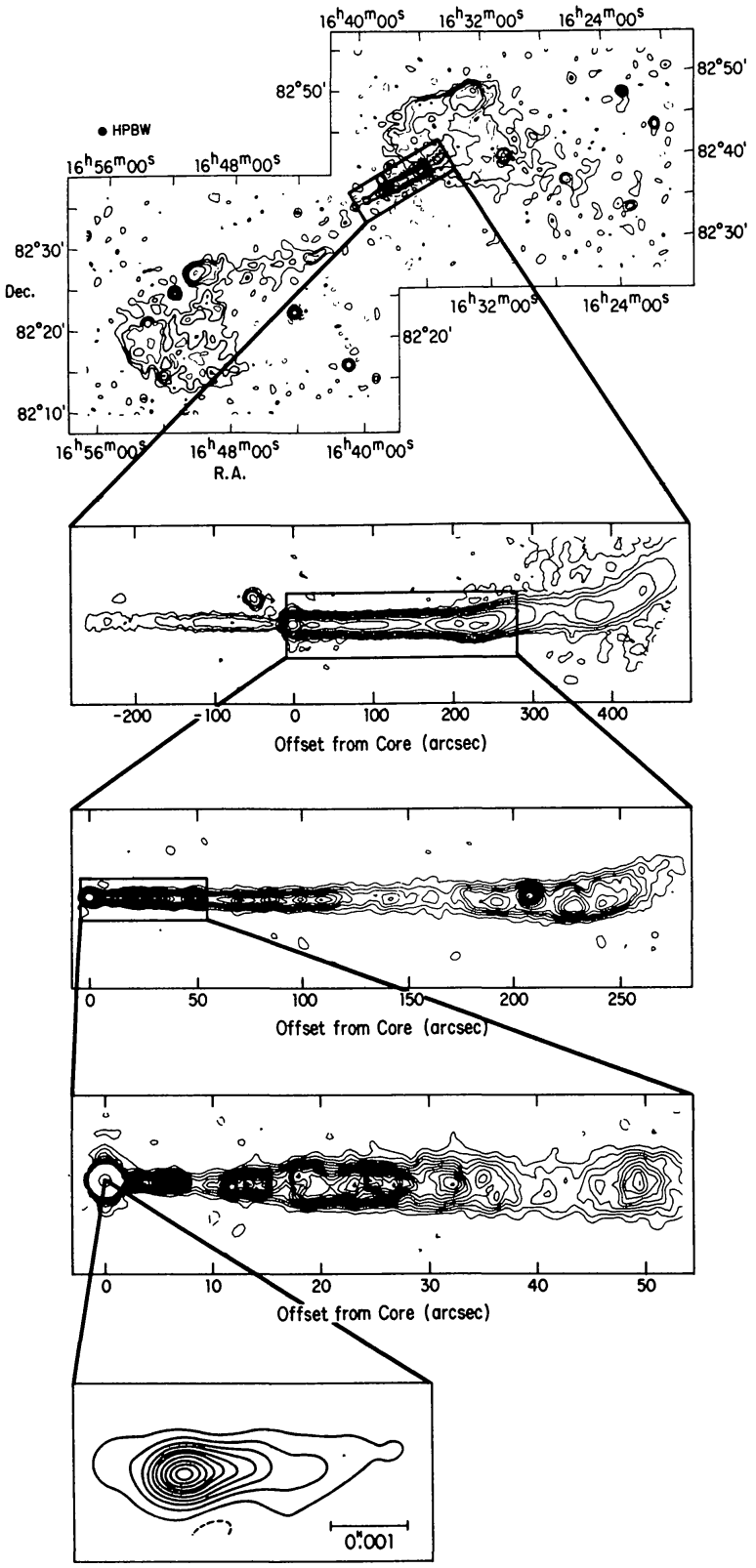

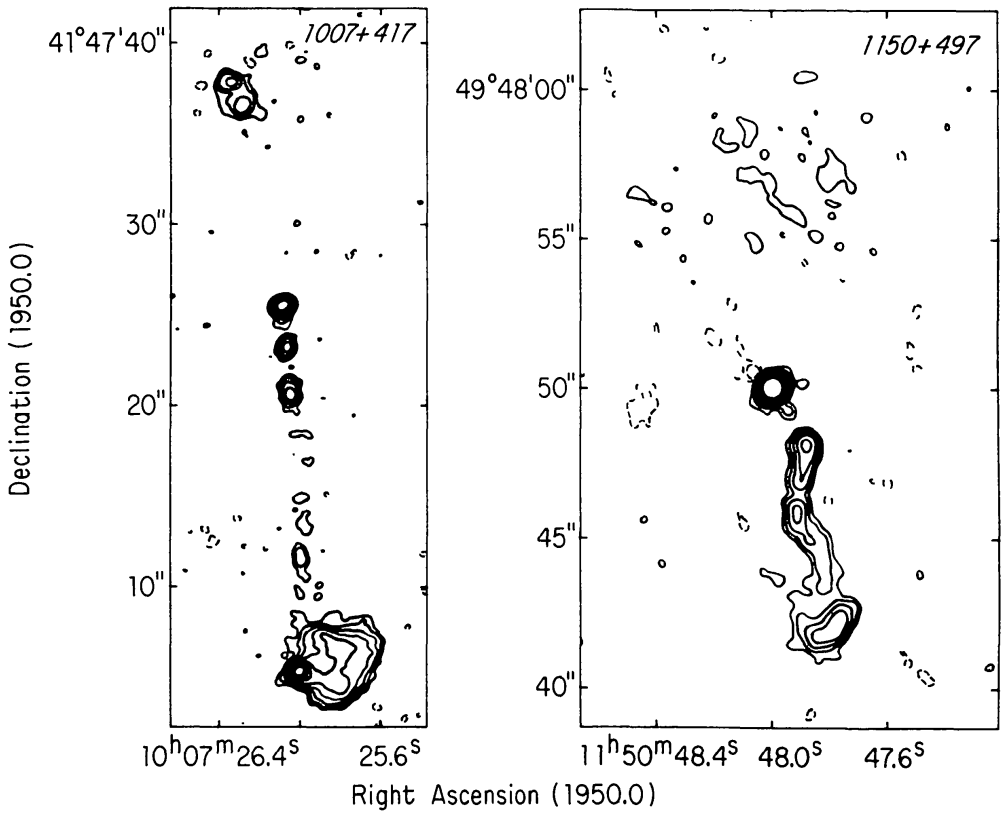


*Figure 3* VLA maps of two one-sided jets in extended QSRs at 4.9 GHz, adapted from (173). Note the knotty structure of the jet in the left panel and the "gap" and the "wiggle" in the jet in the right panel. The peak on each map is the radio core.

from neighboring frequencies, assuming $\nu^0$ spectra for the cores and $\nu^{-0.7}$ for the total emission. Column 5 gives the projected length $d_j$ of the brighter jet in kiloparsecs. Column 6 categorizes the jet sidedness (see Section 3.1). Columns 7 and 8 codify the origin of the data (see the footnotes below the table). We refer to VLBI data on jetlike extensions of the cores in sources with larger-scale jets whether or not the extensions separately meet criterion (1.) of Section 1.2. Table 2 lists 73 sources with features meeting only some of our criteria; modest increases in data quality could promote them to Table 1.

Jets occur in extragalactic sources of all luminosities, sizes, and structure types, always accompanied by detectable emission in the inner kiloparsec of the parent object. It is therefore reasonable to associate jets (*a*) with a

*Figure 2* The structure of the jet and counterjet in NGC 6251 over a wide range of angular scales. Note the knotty substructure of the jet, and the large-scale "wiggle" (*middle panel*). The nuclear "core-jet" (*bottom panel*) and the mean position angle of the larger-scale jet are misaligned by $4.5 \pm 1°$ [data from (279)—top panel; R. A. Perley and A. H. Bridle (in preparation)—second and third panels; (183)—fourth panel; and (56)—bottom panel].

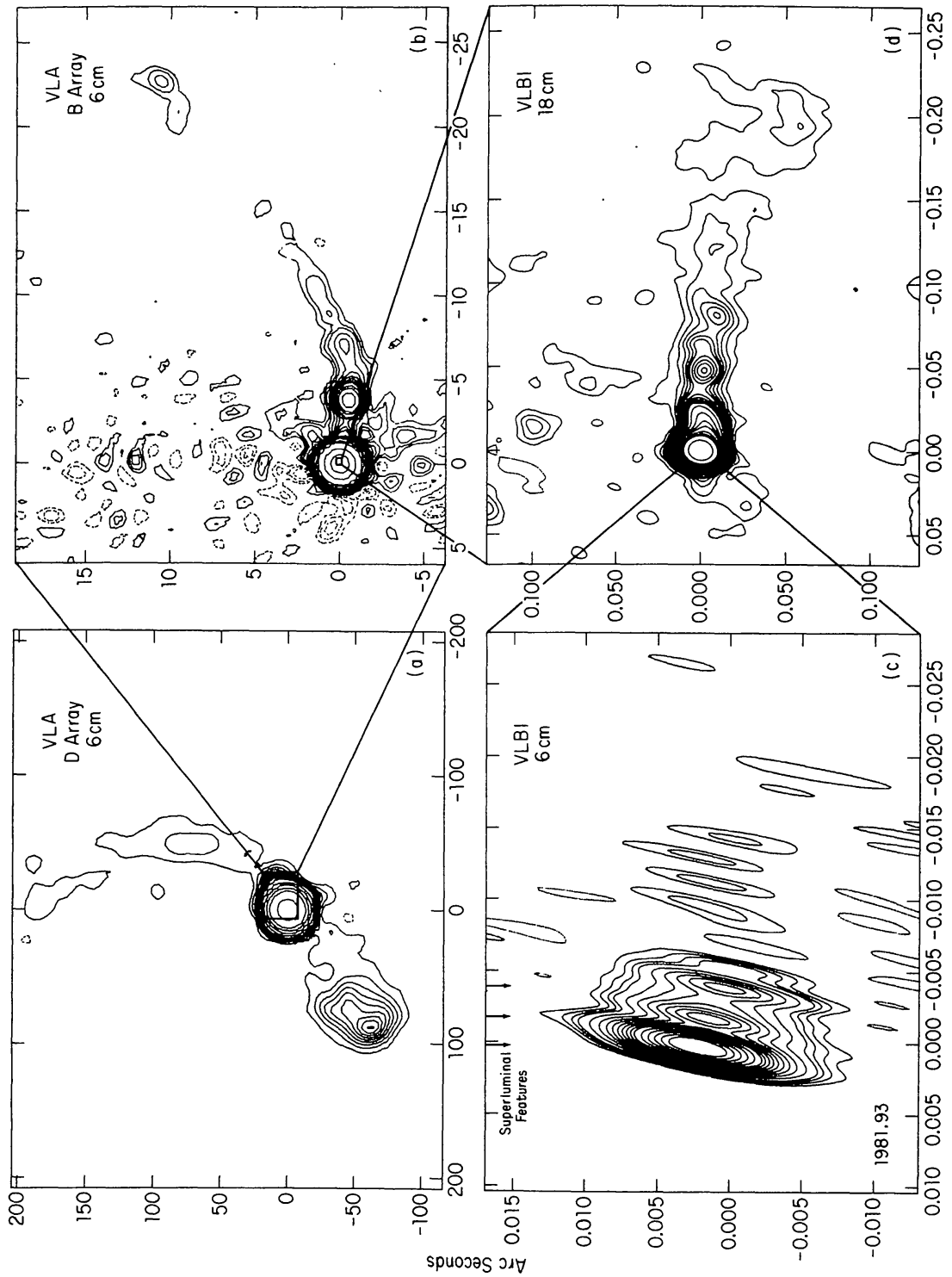


*Figure 4* The structure of the core and jet in 3C 120 over a wide range of angular scales. The three brightest features in the lower-left panel exhibit superluminal expansion (268). Note the continuity between the different scales and the large misalignment between the smallest and largest structures (*left panels*). Montage provided by Drs. R. C. Walker and J. M. Benson.

process common to all extragalactic radio sources and (*b*) with continuing activity in their nuclei. This supports the view that jets result from inefficiencies in the energy transport from the cores to the lobes of extragalactic sources, whether their emission originates in the primary flow itself or in a dissipative sheath around it.

## 2.2 *Occurrence Rates of Jets*

The rates of occurrence of detectable radio jets (by our criteria) can be determined in several samples representing different extragalactic source types.

Twelve (55%) of the 22 radio galaxies in the re-revised 3C sample (140)—

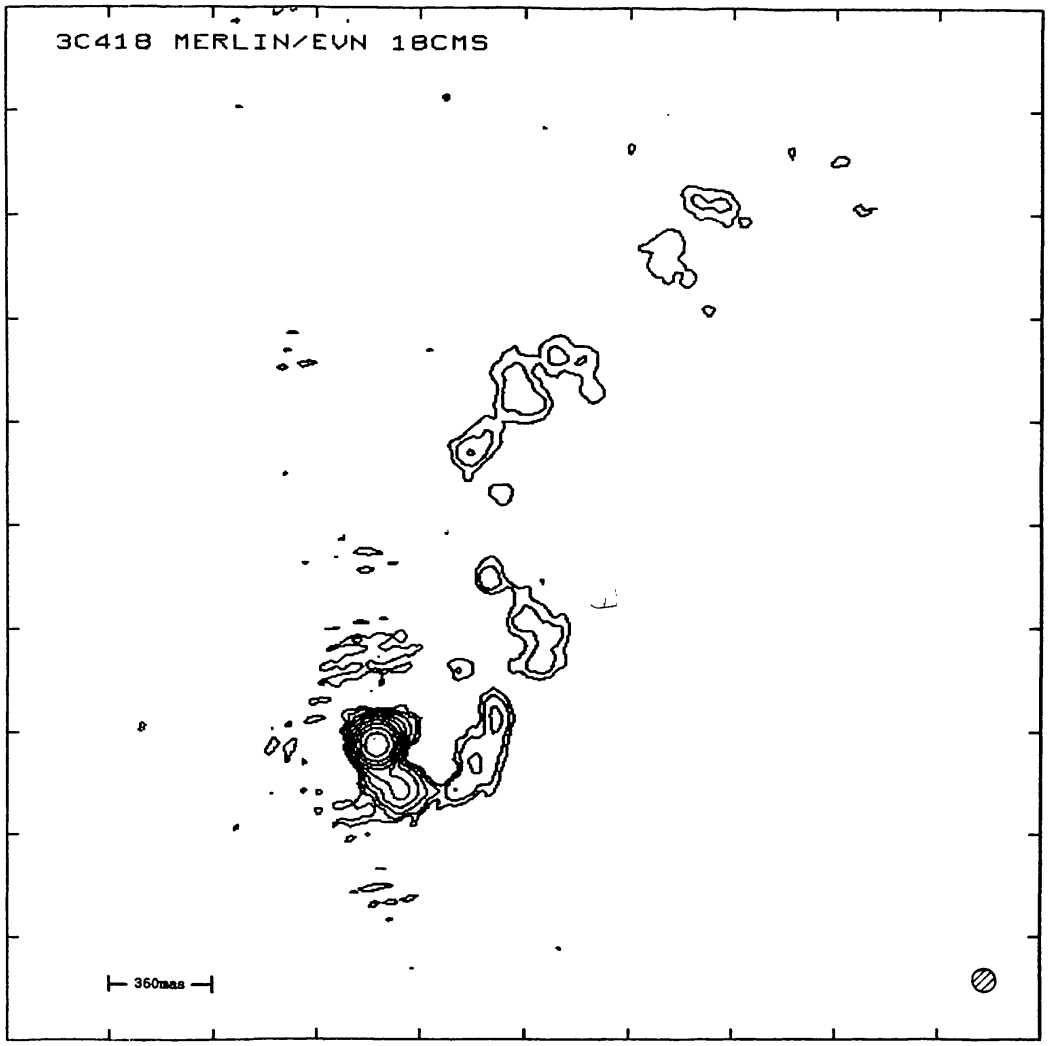


*Figure 5* MERLIN/EVN map of the one-sided jet in the strongly core-dominated QSR 3C 418, provided by Dr. T. B. Muxlow. This is the most powerful core known to be associated with a jet. Note the sharp curvature of the jet near the core and its knotty structure. The tic marks are 0.36″ apart.

**Table 1** 125 extragalactic radio jets

| Source name | ID, $z$ | $P^{5}_{\text{core}}$ | $P^{1.4}_{\text{tot}}$ | $d_j$ | SI | Data[a] | References[b] |
|---|---|---|---|---|---|---|---|
| 0017+15 = 3C 9 | Q, 2.012 | 25.45 | 28.16 | 30. | 1 | A | 248, K1 |
| 0033+18 = 3C 14 | Q, | | | | | A | L4 |
| 0055+30 = NGC 315 | G, 0.0167 | 23.24 | 24.08 | 240 | B | ABW | 27, 29, 30, 99, 142, 278 |
| 0055+26 = NGC 326 | G, 0.0472 | 22.29 | 24.61 | 25. | 2 | AW | 97 |
| 0104+32 = 3C 31 (NGC 383) | G, 0.0169 | 22.45 | 24.21 | 14. | 2 | ACOW | 32, 42, 52, 99, 245 |
| 0106+72 = 3C 33.1 | G, 0.181 | 23.76 | 26.11 | 140 | 1 | AW | 258, R1 |
| 0123−01 = 3C 40 | G, 0.018 | 22.35 | 24.38 | 38. | 2 | A | O1 |
| 0130+24 = 4C 24.02 | Q, 0.457 | 25.11 | 26.21 | 92. | ? | A | W1 |
| 0149+35 = NGC 708 | G, 0.0160 | 21.31 | 22.62 | 4.5 | 2 | A | D1, L3 |
| 0206+35 = UGC 1651 | G, 0.0373 | 23.15 | 24.52 | 18. | 2 | A | D1, L3 |
| 0220+42 = 3C 66B | G, 0.0215 | 22.59 | 24.69 | 45. | 2 | ACOW | 52, 168, 258 |
| 0238+08 = NGC 1044 | G, 0.0214 | 22.54 | 23.80 | 43. | 2 | AN | 100, C1 |
| 0240−00 = 3C 71 (NGC 1068) | G, 0.004 | 20.99 | 22.94 | 0.3 | 2 | ABM | 62, 180, 264, 282, 283 |
| 0255+05 = 3C 75A,B | G, 0.0241 | 22.40 | 24.61 | 30. | 2 | A | O2 |
| 0256+13 = 4C 13.17B | G, 0.0748 | 22.30 | 24.07 | 15. | 2 | A | O1 |
| 0305+03 = 3C 78 (NGC 1218) | G, 0.0289 | 23.77 | 24.83 | 0.6 | 1 | ABM | 126, P2, U1 |
| 0314+41 = 3C 83.1B (NGC 1265) | G, 0.0255 | 22.15 | 24.76 | 18. | 2 | ACW | 161, 171, 272 |
| 0316+41 = 3C 84 (NGC 1275) | G, 0.0177 | 24.87 | 24.66 | 5.0 | 1 | BM | 176, 179, 200 |
| 0320−37 = For A (NGC 1316) | G, 0.0063 | 21.23 | 24.69 | 2.7 | B | A | 96 |
| 0326+39 = VV 7.08.14 | G, 0.0243 | 22.70 | 24.06 | 41. | 2 | AW | 27, 174 |
| 0336−35 = PK (NGC 1399) | G, 0.0049 | 20.41 | 22.71 | 8.1 | 2 | A | E1 |
| 0415+37 = 3C 111 | G, 0.0485 | 24.47 | 25.59 | 78. | 1 | AB | 97, 142, 145 |
| 0430+05 = 3C 120 | G, 0.0334 | 24.93 | 24.76 | 83. | 1 | ABMW | 2, 5, 6, 38, 126, 224, 268, 269 |
| 0445+44 = 3C 129 | G, 0.0208 | 22.19 | 24.58 | 8.8 | B | ACW | 44, 214, 258, 262 |
| 0449−17 = PK | G, 0.0313 | 22.03 | 23.93 | 10. | 2 | A | E1 |
| 0459+25 = 3C 133 | G, 0.2775 | 25.33 | 26.72 | 14. | 1 | AM | 138, 212, L1 |
| 0514−16 = PK | Q, 1.278 | 27.32 | 27.25 | 33. | 1 | A | P2 |
| 0538+49 = 3C 147 | Q, 0.545 | 26.78 | 27.95 | 0.8 | 1 | BM | 193, 194, 201, 203, 233, 234, 275 |
| 0546−32 = PK | G, 0.147 | 23.90 | 25.47 | 200 | ? | A | E1 |

1984ARA&A..22..319B



| | | | | | | | |
|---|---|---|---|---|---|---|---|
| 0658+33 = B2 | G, 0.127 | 23.98 | 24.82 | 55. | 2 | A | O1 |
| 0704+35A = 4C 35.16A | G, 0.078 | 21.83 | 24.28 | 17. | 2 | A | O1 |
| 0712+53 = 4C 53.16 | G, 0.064 | 22.96 | 24.83 | 13. | ? | A | 49 |
| 0723+67 = 3C 179 | Q, 0.846 | 26.62 | 27.39 | 18. | 1 | ABM | 38, 173 |
| 0742+31 = 4C 31.30 | Q, 0.462 | 26.24 | 26.55 | 210 | 1 | A | 163 |
| 0812+36 = B2 | Q, 1.025 | 27.10 | 27.23 | 30. | 1 | A | 185, P2 |
| 0812+02 = 4C 02.23 | Q, 0.402 | 25.60 | 26.68 | 32. | ? | A | 102, 285, H1 |
| 0824+29 = 3C 200 | G, 0.458 | 24.98 | 26.73 | 41. | 1 | A | B2 |
| 0833+65 = 3C 204 | Q, 1.112 | 25.71 | 27.39 | 52. | 1 | A | L1 |
| 0833+58 | Q, 2.101 | 27.64 | 27.52 | 45. | ? | A | P2 |
| 0838+13 = 3C 207 | Q, 0.684 | 26.45 | 27.23 | 25. | 1 | A | W1 |
| 0844+31 = 4C 31.32 | G, 0.0675 | 23.35 | 24.88 | 61. | ? | AW | 258, 262 |
| 0850+14 = 3C 208 | Q, 1.11 | 26.44 | 27.64 | 22. | ? | A | L1 |
| 0855+14 = 3C 212 | Q, 1.049 | 25.38 | 27.61 | 22. | 1 | A | L1 |
| 0908+37 = B2 | G, 0.1047 | 23.50 | 24.89 | 23. | 2 | A | 153, D1 |
| 0917+45 = 3C 219 | G, 0.1744 | 24.18 | 26.45 | 36. | 1 | ACNW | 184, 253 |
| 0938+39 = 4C 39.27 | Q, 0.618 | 25.00 | 26.99 | 96. | 1 | A | 190, W1 |
| 0957+00 = 4C 00.34 | Q, 0.907 | 26.02 | 27.03 | 76. | ? | A | H1 |
| 0957+56 = Double QSO | Q, 1.405 | 26.28 | 27.15 | 22. | 1 | AB | 108, 109, 189 |
| 1001+22 = 4C 22.26 | Q, 0.974 | 25.73 | 26.94 | 31. | ? | A | W1 |
| 1003+35 = 3C 236 | G, 0.0989 | 24.64 | 25.78 | 0.4 | 1 | A(?)B | 98, 225 |
| 1004+14 = NGC 3121 | G, 0.031 | 22.97 | 24.07 | 77. | 2 | AC | 125, C1 |
| 1004+13 = 4C 13.41 | Q, 0.240 | 23.87 | 25.92 | 60. | 1 | A | 96 |
| 1007+41 = 4C 41.21 | Q, 0.613 | 25.86 | 26.91 | 77. | 1 | A | 173 |
| 1029+57 = HB 13 | G, 0.034 | 22.50 | 23.70 | 280 | 2 | CW | 156, S2 |
| 1033+00 = PK | G, | | | | | A | 216 |
| 1100+77 = 3C 249.1 | Q, 0.311 | 25.00 | 26.41 | 21. | 1 | A | 149, B2, L1 |
| 1122+39 = NGC 3665 | G, 0.0067 | 20.46 | 21.76 | 3.9 | 2 | A | D1, H2 |
| 1131+49 = IC 708 | G, 0.0321 | 22.74 | 24.13 | 35. | 2 | A | 257 |
| 1137+18 = NGC 3801 | G, 0.0105 | 20.59 | 23.06 | 2.1 | 2 | AC | 125, L1 |
| 1150+49 = 4C 49.22 | Q, 0.334 | 25.88 | 26.43 | 23. | 1 | A | 173, 181 |
| 1209+74 = 4C T.74.17.1 | G, 0.107 | 23.26 | 24.99 | 120 | 1 | AW | 263, P2 |
| 1216+06 = 3C 270 (NGC 4261) | G, 0.0073 | 22.25 | 24.01 | 31. | 2 | A | 126, K1 |

**Table 1** (*continued*)

| Source name | ID, $z$ | $P^{5}_{\text{core}}$ | $P^{1.4}_{\text{tot}}$ | $d_j$ | SI | Data[a] | References[b] |
|---|---|---|---|---|---|---|---|
| 1217+02 = PK | Q, 0.240 | 25.33 | 25.68 | 120 | ? | A | 163 |
| 1222+13 = 3C 272.1 (M84) | G, 0.0031 | 21.72 | 23.24 | 3.3 | 2 | ABCW | 126, 127, L2 |
| 1226+02 = 3C 273 | Q, 0.158 | 26.92 | 27.12 | 39. | 1 | ABMOX | 2, 38, 58, 64, 175, 178, 181, 199, 226, P2 |
| 1228+12 = Vir A (M87) | G, 0.0043 | 22.92 | 24.78 | 1.8 | 1 | ABCMOX | 1, 2, 18, 54, 67, 71, 135, 141, 150, 164, 165, 172, 209, 226, 230, 237, 244, 247, 249 |
| 1241+16 = 3C 275.1 | Q, 0.557 | 25.74 | 27.08 | 36. | ? | A | 243 |
| 1250−10 = NGC 4760 | G, 0.0138 | 22.14 | 23.27 | 2.9 | 2 | A | L1 |
| 1251+273 = NGC 4789 | G, 0.027 | 21.16 | 23.55 | 6.7 | 2 | A | L3 |
| 1251+278 = 3C 277.3 (Com A) | G, 0.0857 | 22.98 | 25.37 | 11. | 1 | AO | 31, 158, 159, V3 |
| 1251−12 = 3C 278 (NGC 4783) | G, 0.0138 | 22.13 | 24.23 | 14. | 2 | A | C1 |
| 1253−05 = 3C 279 | Q, 0.536 | 27.56 | 27.53 | 9.9 | 1 | AB | 38, 70, 175 |
| 1256+28 = NGC 4869 | G, 0.0235 | 21.08 | 22.89 | 2.6 | ? | A | O1 |
| 1258+40 = 3C 280.1 | Q, 1.659 | 26.21 | 27.84 | 42. | 1 | A | 248 |
| 1258−32 = PK | G, | | | | | A | P2 |
| 1315+34 = B2 | Q, 1.050 | 26.76 | 26.98 | 13. | 1 | A | 181 |
| 1316+29 = 4C 29.47 | G, 0.728 | 23.25 | 24.85 | 110 | 2 | A | 63 |
| 1317+52 = 4C 52.27 | Q, 1.060 | 26.79 | 27.37 | 60. | ? | A | 173, H1 |
| 1321+31 = NGC 5127 | G, 0.0161 | 21.77 | 23.85 | 55. | 2 | ACW | 83, 88, 125 |
| 1322−42 = Cen A (NGC 5128) | G, 0.0012 | 22.20 | 24.62 | 5.2 | 1 | ABOX | 20, 34, 48, 77, 91, 106, 107, 170, 187, 188, 192, 228, 229, 235 |
| 1328+30 = 3C 286 | Q, 0.849 | 27.88 | 28.18 | 0.2 | ? | AB | 177, 234, P1 |
| 1333−33 = IC 4296 | G, 0.0129 | 22.46 | 24.05 | 128 | 2 | A | 103, E1 |
| 1407+17 = NGC 5490 | G, 0.0163 | 22.00 | 23.68 | 5.5 | 2 | C | 125 |
| 1414+11 = 3C 296 (NGC 5532) | G, 0.0237 | 22.67 | 24.43 | 50. | 2 | AC | 19, L1 |
| 1441+52 = 3C 303 | G, 0.141 | 24.53 | 25.75 | 26. | ? | A | 148, K1 |
| 1448+63 = 3C 305 | G, 0.041 | 22.57 | 24.73 | 0.9 | 2 | A | 116 |
| 1450+28 = B2 | G, 0.1265 | 22.56 | 24.56 | 37. | 2 | A | D1 |
| 1451−37 = PK | Q, 0.314 | 26.24 | 26.36 | 17. | 1 | A | 181 |
| 1458+71 = 3C 309.1 | Q, 0.904 | 27.62 | 28.01 | 3.8 | ? | BM | 274, S1 |

| | | | | | | | |
|---|---|---|---|---|---|---|---|
| 1615+42 | G, 0.131 | 23.20 | 24.20 | 14. | 2 | A | O1 |
| 1618+17 = 3C 334 | Q, 0.555 | 25.78 | 26.97 | 63. | ? | A | 271, H1 |
| 1626+27 = 3C 341 | G, 0.448 | 23.49 | 26.80 | 112 | B | A | This paper, Figure 6 |
| 1637+82 = NGC 6251 | G, 0.0230 | 23.66 | 24.14 | 161 | 1 | ABCW | 33, 56, 183, 198, 220, 267, 280 |
| 1638+53 = 4C 53.37 | G, 0.1098 | 23.21 | 24.93 | 40. | 2 | A | 45, 50 |
| 1641+39 = 3C 345 | Q, 0.594 | 27.62 | 27.52 | 9.5 | 1 | AB | 38, 58–60, 177, 199, 200, 224, 241, 255, P2 |
| 1642+69 = 4C 69.21 | Q, | | | | | M | 39 |
| 1648+05 = 3C 348 (Her A) | G, 0.154 | 23.61 | 27.10 | 118 | 1 | A | D2 |
| 1752+32 = B2 1752+32B | G, 0.0449 | 22.67 | 23.46 | 30. | 2 | A | D1 |
| 1759+21 = PK | G, | | | | | A | 216 |
| 1807+27 = 4C 27.41 | Q, 1.76 | 27.29 | 27.66 | 13. | ? | A | P2 |
| 1807+69 = 3C 371 | G, 0.050 | 24.60 | 24.84 | 2.0 | 1 | AB | 39, 176, P1 |
| 1842+45 = 3C 388 | G, 0.0908 | 23.76 | 25.73 | 18. | 1 | A | 46, 47 |
| 1857+56 = 4C 56.28 | Q, 1.595 | 26.34 | 27.57 | 62. | 1 | A | 173, 216, 217 |
| 1919+47 = 4C 47.51 | G, 0.103 | 23.19 | 24.86 | 265 | 1 | A | 43, 211 |
| 1924+50 = 4C 50.47 | Q, | | | | | A | 173 |
| 1939+60 = 3C 401 | G, 0.201 | 24.14 | 26.37 | 24. | 1 | A | B2, L1 |
| 1940+50 = 3C 402N | G, 0.0247 | 22.08 | 24.31 | 6.2 | 2 | C | 210 |
| 1957+40 = 3C 405 (Cyg A) | G, 0.057 | 24.12 | 27.73 | 47. | ? | AB | 132, 142, P2 |
| 2037+51 = 3C 418 | Q, 1.686 | 28.24 | 28.41 | 9.3 | 1 | ABM | 274, M1 |
| 2116+26 = NGC 7052 | G, 0.0164 | 22.12 | 22.72 | 26. | 2 | A | 125, D1, L3 |
| 2121+24 = 3C 433 | G, 0.1016 | 22.76 | 26.15 | 30. | ? | A | 259 |
| 2153+37 = 3C 438 | G, 0.292 | 23.99 | 26.86 | 27. | 2 | A | L1 |
| 2221−02 = 3C 445 | G, 0.057 | 23.51 | 25.30 | 210 | 1 | A | V1 |
| 2229+39 = 3C 449 | G, 0.0171 | 22.07 | 24.03 | 19. | 2 | ACW | 19, 65, 186, P2 |
| 2236+35 = B2 | G, 0.0277 | 21.88 | 23.40 | 7.7 | 2 | A | D1 |
| 2251+15 = 3C 454.3 | Q, 0.859 | 28.02 | 28.10 | 21. | 1 | AM | 38, 177, 181, 274 |
| 2300−18 = PK | Q, 0.129 | 24.90 | 25.45 | 68. | 1 | A | 122 |
| 2316+18 = OZ 127 | G, 0.0395 | 22.41 | 23.70 | 16. | 2 | A | O1 |
| 2318+07 = NGC 7626 | G, 0.0112 | 21.31 | 23.17 | 6.4 | 2 | A | L1 |
| 2325+29 = 4C 29.68 | Q, 1.015 | 26.37 | 27.34 | 85. | ? | A | W1 |
| 2335+26 = 3C 465 (NGC 7720) | G, 0.0293 | 23.37 | 24.85 | 24. | 1 | ACW | 44, 81, 258 |
| 2337+26 = NGC 7728 | G, 0.0314 | 23.15 | 23.49 | 39. | 2 | ACW | 125, 126, 127, L1, V2 |

**Table 1** (*continued*)

| Source name | ID, $z$ | $P^{5}_{\text{core}}$ | $P^{1.4}_{\text{tot}}$ | $d_j$ | SI | Data[a] | References[b] |
|---|---|---|---|---|---|---|---|
| 2338+04 = 4C 04.81 | Q, 2.594 | 27.15 | 27.98 | 4.6 | ? | M | B1 |
| 2349+32 = 4C 32.69 | Q, 0.671 | 25.15 | 26.57 | 99. | 1 | A | 75, 190, 191, 271 |
| 2354+47 = 4C 47.63 | G, 0.046 | 22.49 | 24.63 | 37. | 1 | A | 49 |

[a] Data codes: A—VLA; B—VLB; C—Cambridge; M—MERLIN; N—NRAO; O—optical; X—X-ray; W—WSRT.

[b] Unpublished references:

B1: Barthel, P. D., Lonsdale, C. J. 1983. Preprint
B2: Burns, J. O., Basart, J. P., De Young, D. S., unpublished data
C1: Cornwell, T. J., unpublished data
D1: de Ruiter, H., Parma, P., Fanti, C., Fanti, R., unpublished data
D2: Dreher, J. W., Feigelson, E. D. 1983. Preprint
E1: Ekers, R. D., unpublished data
H1: Hintzen, P., Ulvestad, J., Owen, F. N. 1983. Preprint
H2: Hummel, E., Kotanyi, C., unpublished data
K1: Kronberg, P. P., unpublished data
L1: Laing, R. A., unpublished data
L2: Laing, R. A., Bridle, A. H., unpublished data
L3: Laing, R. A., Kotanyi, C., Hummel, E., unpublished data
L4: Laing, R. A., Owen, F. N., Puschell, J., unpublished data
M1: Muxlow, T. W. B., Jullian, M., Linfield, R., unpublished data
O1: O'Dea, C. P., unpublished data
O2: Owen, F. N., unpublished data
P1: Pearson, T. J., Perley, R. A., Readhead, A. C. S., unpublished data
P2: Perley, R. A., unpublished data
R1: Rudnick, L., Edgar, B. K., unpublished data
S1: Simon, R. S., unpublished data
S2: Strom, R. G., unpublished data
U1: Unger, S. V., Booler, R. V., Pedlar, A. 1983. Preprint
V1: van Breugel, W. J. M., unpublished data
V2: van Breugel, W. J. M., Fomalont, E. B., Bridle, A. H., unpublished data
V3: van Breugel, W. J. M., Miley, G. K., Heckman, T., Butcher, H. R., Bridle, A. H., unpublished data
W1: Wardle, J. F. C., Potash, R. I., Roberts, D. H., unpublished data.

henceforth 3CR[2]—with $\delta \geq 10°$, $b \geq 10°$, and $z \leq 0.05$ have definite jets, and two more (9%) have possible jets. We exclude from the sample the weak source 3C 231 = M82, whose emission comes mainly from a galactic disk. A fifteenth galaxy (3C 338) has structure resembling a jet except that it does not align with the radio core (51). Jets are thus detected in at least 55%, and perhaps 65%, of this sample, whose median $P_{\rm tot}^{1.4}$ is $10^{24.43}$ W Hz$^{-1}$. Jets were also found in 82% (9 of 11) of well-resolved sources in a complete sample of B2 radio galaxies with $m_{\rm pg} < 15.7$ (83). R. A. Laing (private communication) finds definite jets in 13 sources (55%), and possible jets in 5 more (20%), in an unbiased sample of 24 E and S0 galaxies with $0° < \delta < 37°$, $m_{\rm pg} \leq 14.0$, and $S_{\rm tot}^{2.3} > 0.035$ Jy.

Forty-two extended 3CR[2] galaxies or probable galaxies with $z > 0.4$ or $V > 20$ have been mapped at the VLA with good dynamic range (Table 1, ref. L4). Only two (5%) of these powerful radio galaxies (median $P_{\rm tot}^{1.4} = 10^{27.36}$ W Hz$^{-1}$) have continuous jets; one other has an elongated knot between its core and one lobe.

Twenty-two extended 3CR[2] QSRs have been mapped at the VLA with

**Table 2** 73 possible extragalactic radio jets

| | | |
|---|---|---|
| 0120+33 = NGC 507 | 0913+38 = B2 | 1508−05 = 4C −05.64 |
| 0131−36 = NGC 612 | 0915−11 = 3C 218 (Hyd A) | 1510−08 = PK |
| 0134+32 = 3C 48 | 0926+79 = 3C 220.1 | 1529+24 = 3C 321 |
| 0137+01 = 4C 01.04 | 0947+14 = 3C 228 | 1548+114 = 4C 11.50 |
| 0212+17 = MC 3 | 0956−26 = NGC 3078 | 1615+35 = NGC 6109 |
| 0300+16 = 3C 76.1 | 1015+49 | 1626+39 = 3C 338 (NGC 6166) |
| 0327+24 = B2 | 1103−00 = 4C −00.43 | 1636+47 |
| 0333+32 = NRAO 140 | 1104+16 = 4C 16.30 | 1704+60 = 3C 351 |
| 0448+51 = 3C 130 | 1108+27 = B2 | 1712+63 |
| 0457+05 | 1113+29 = 4C 29.41 | 1850+70 |
| 0518+16 = 3C 138 | 1144+35 = B2 | 1828+48 = 3C 380 |
| 0531−36 | 1208+39 = NGC 4151 | 1830+28 = 4C 28.45 |
| 0549−07 = NGC 2110 | 1218+33 = 3C 270.1 | 1833+32 = 3C 382 |
| 0609+71 = Markarian 3 | 1222+21 = 4C 21.35 | 1845+79 = 3C 390.3 |
| 0634−20 = MSH 06−210 | 1254+27 = NGC 4839 | 1928+73 |
| 0703+42 = 4C 42.23 | 1317+25 = 4C 25.42 | 2019+09 = 3C 411 |
| 0716+71 | 1319+64 = 4C 64.18 | 2040−26 = PK |
| 0722+30 = B2 | 1336+39 = 3C 288 | 2201+31 = 4C 31.63 |
| 0754+12 | 1346+26 = 4C 26.42 | 2203+29 = 3C 441 |
| 0755+37 = NGC 2484 | 1347+60 = NGC 5322 | 2216−03 = 4C −03.79 |
| 0802+10 = 3C 191 | 1350+31 = 3C 293 | 2223−05 = 3C 446 |
| 0814+54 = 4C 54.16 | 1351+36 = NGC 5352 | 2247+11 = NGC 7385 |
| 0837+29 = 4C 29.30 | 1404+34 = 3C 294 | 2305+18 = 4C 18.08 |
| 0903+16 = 3C 215 | 1415+25 = NGC 5548 | |
| 0905−09 = 26W20 | 1419+41 = 3C 299 | |

good dynamic range (Table 1, refs. L4 and W1). Ten (45%) of this group (whose median $P_{tot}^{1.4}$ is $10^{27.43}$ W Hz$^{-1}$, similar to that of the distant 3CR[2] galaxies) have definite jets, and five more (23%) have structure resembling the brighter parts of jets. Ten (40%) of 24 extended QSRs in a 966-MHz survey have jets or structure resembling them (173), while five of the eight most extended sources in a complete sample of 4C QSRs have jets (271).

Jets are thus detected in 65 to 80% of weak radio galaxies, and in 40 to 70% of extended QSRs, but (with similar instrumental parameters) in only $< 10\%$ of distant galaxies similar to the QSRs in radio power (49, 139, 173). Among the extended 3CR[2] QSRs, the jet detection rate increases with the relative prominence $f_C = S_{core}^{5}/S_{tot}^{1.4}$ of the radio core, apparently regardless of redshift: all six QSRs with $f_C > 0.03$ (but only two of the six with $f_C < 0.005$) have jets or features resembling the brightest parts of jets. The lack of detectable jets in distant 3CR[2] galaxies may be related to their lower values of $f_C$—the median $f_C$ in the distant 3CR[2] galaxy sample is only 0.0005. The two with detected jets are 3C 200, with $f_C = 0.018$ and weak emission lines, and 3C 341 (Figure 6), with $f_C = 0.0005$ and strong emission lines. The relations between jet, core, and emission-line fluxes of 3CR[2] galaxies need clarifying, but the multivariate ($P_{tot}$, $P_{core}$, $P_{optical}$) luminosity function for radio jets may contain clues to the physics of energy transport in these sources. We urge observers to publish integrated flux densities of jets and lobes separately, to allow study of this function.

## 2.3 *Jets in Weak Sources?*

2.3.1 SPIRAL GALAXIES Several Seyfert galaxies (for a review and references, see 282) with $10^{21.5} < P_{tot}^{1.4} < 10^{23}$ W Hz$^{-1}$ have S-shaped kiloparsec-scale radio structures that may be low-thrust jets being bent and disrupted by the ram pressure of a rotating gas disk. If this is correct, the radio sources in Seyfert spirals may differ from those in ellipticals and QSRs mainly by (*a*) the smaller power output of the central "engine" and (*b*) the

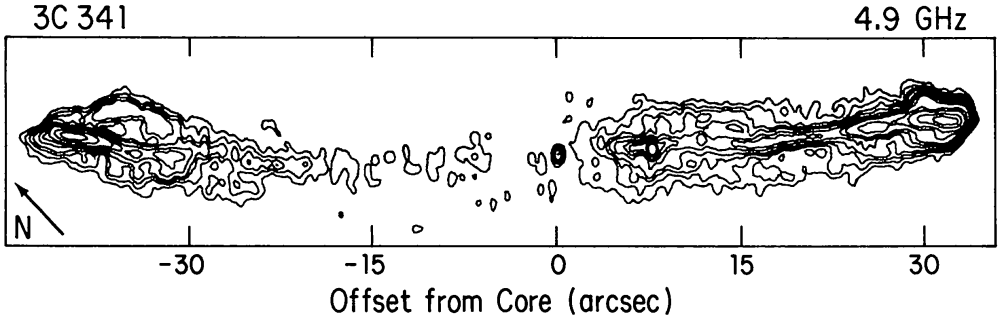


*Figure 6* VLA map of the jets and cocoon in the distant radio galaxy 3C 341 at 4.9 GHz. Note the narrowing of the cocoon to the right of the figure, and the irregular brightness distribution of the jets (data of A. H. Bridle and E. B. Fomalont, in preparation).

inability of their jets to escape from the dense, rotating interstellar medium (ISM) of a spiral disk. Interpreting the Seyfert sources as continuous jets (282) is not yet obligatory, however (264). Several edge-on spirals with unusually bright compact cores (121, and references therein) also have radio features extending from their nuclei apparently near the galactic minor axes. The features are as yet too poorly resolved to meet our criteria for jethood (Section 1.2), but if they do result from nuclear activity, they could be weak analogs of jets in elliptical galaxies.

2.3.2 GALACTIC JETS The S-shaped structure of Sgr A West (36, 84) and its relation to the velocities of the [Ne II] lines in the region can be interpreted as the result of collimated outflow from the galactic center at $\sim 300$ km s$^{-1}$ (35, 84). The extent to which Sgr A West is a weak parsec-scale analog of more active galactic nuclei is unclear, however; the S-structure has a thermal spectrum (unlike extragalactic jets; Section 4.2), and models involving tidal distortion of infalling clouds also fit the data (84). The binary star SS 433 has the only astrophysical jet whose velocity ($0.26c$) and precessional geometry relative to us are unambiguous (for reviews and references, see 120, 154). Both the $\sim 100$ light-day scale of the known radio structure and its typical radio luminosity ($P_{\rm tot}^{1.4} = 10^{15.8}$ W Hz$^{-1}$) are much less than those of extragalactic jets, but SS 433 allows us to observe the evolution of synchrotron-emitting plasma in precessing supersonic jets directly. There is also evidence for bipolar, and perhaps well-collimated, outflows from star-forming regions in dense molecular clouds—see (55) and (232) for reviews and references. The ability to measure velocities, densities, and temperatures in and around these nearby flows may help to test models of extragalactic jet production and propagation (133, 207).

# 3. TRENDS WITH LUMINOSITY

## 3.1 *Sidedness*

Most extended extragalactic sources have lobes of similar powers and sizes on each side of the parent object, but not all jets have detectable counterjets. We denote by $\mathcal{S}$ the ratio of intensities between the brighter and fainter jet measured at the same distance from the parent object at low transverse resolution (to minimize the influence on $\mathcal{S}$ of differences in their expansion rates). We classify as *one sided* those for which $\mathcal{S} > 4$ wherever the dynamic range of the map allows this to be determined, and as *two sided* those for which $\mathcal{S} < 4$ everywhere. We use $\mathcal{S} = 4$ as the break point solely because it separates two equally numerous groups of jets on available maps, not because it has special physical meaning.

Most jets are one-sided close to their parent object. Jets in weak radio

galaxies (e.g. Figure 1) become two sided after a few kiloparsecs; the one-sided bases are typically $<10\%$ of their length, and the jet with the one-sided base is generally somewhat brighter on the large scale. Table 1 (Column 6) classifies the sidedness of the outer 90% of the jets—"1" if $\mathcal{S} > 4$, "2" if $\mathcal{S} < 4$, and "B" if $\mathcal{S} > 4$ at some distances from the core but $\mathcal{S} < 4$ at others. Most jets in sources with $P^5_{\rm core} \leq 10^{23}$ W Hz$^{-1}$ or $P^{1.4}_{\rm tot} \leq 10^{24.5}$ W Hz$^{-1}$ are mainly two sided, while most jets in more powerful sources, whether radio galaxies or QSRs, are entirely one sided. The value $P^{1.4}_{\rm tot} \approx 10^{25}$ W Hz$^{-1}$ marks the transition between the structural classes I and II of Fanaroff & Riley (86; henceforth FR): the jets in FR I sources (weak, edge darkened, lacking hot spots) are mainly two sided, while those in FR II sources (powerful, edge brightened, strong hot spots) are one sided. All jets in QSRs, whether core dominated or lobe dominated, are entirely one sided.

## 3.2 *Magnetic Configuration*

Degrees of linear polarization up to 40% are common in radio jets at centimeter wavelengths (e.g. 19, 99, 186, 191, 220, 248, 263), and local values $>50\%$ are not unusual (183, 184, 256, 278). Jets with low ($<5\%$) polarization at centimeter wavelengths (31, 47) are exceptional. High degrees of polarization imply ordering of the component of the jet magnetic field $\mathbf{B}_j$ perpendicular to the line of sight, but this order need not be three dimensional (137). Field ordering is seen directly on well-resolved maps of the "apparent" (synchrotron emissivity weighted) field $\mathbf{B}_a$ derived from multifrequency polarimetry. Three magnetic configurations are common in the 40 jets for which adequate polarimetry exists:

1. $B_{\parallel}$, i.e. $\mathbf{B}_a$ is predominantly parallel to the jet axis all across the jet.
2. $B_{\perp}$, i.e. $\mathbf{B}_a$ is predominantly perpendicular to the jet axis all across it.
3. $B_{\perp\text{-}\parallel}$, i.e. $\mathbf{B}_a$ is predominantly perpendicular to the jet axis at the center of the jet, but becomes parallel to the axis near one or both of its edges.

Most two-sided regions of straight jets have either the $B_{\perp}$ or the $B_{\perp\text{-}\parallel}$ field configuration, while most one-sided regions of jets have the $B_{\parallel}$ configuration (27, 277). In most straight jets in sources with $P^5_{\rm core} < 10^{23}$ W Hz$^{-1}$ (or $P^{1.4}_{\rm tot} < 10^{24.5}$ W Hz$^{-1}$), $\mathbf{B}_a$ turns from $B_{\parallel}$ to $B_{\perp}$ or $B_{\perp\text{-}\parallel}$ in the first 10% of the jet, but most jets in more powerful sources are $B_{\parallel}$-dominated for their entire length (27, and A. H. Bridle, in preparation). This observation, in combination with those of Section 3.1, identifies two main classes of (straight) radio jet—two-sided $B_{\perp}$- or $B_{\perp\text{-}\parallel}$-dominated jets in weak FR I sources (edge darkened, no hot spots) and one-sided $B_{\parallel}$-dominated jets in powerful FR II sources (edge brightened, stronger hot spots).

Two departures from this trend may arise when jet flows are perturbed:

1. Two-sided jets often have the $B_{\perp\text{-}\parallel}$ configuration where they bend. The $B_{\parallel}$ edge is often deeper (and more strongly polarized) on the outside of the bend [e.g. 3C 31 (42, 245), NGC 6251 (183), M84 (Table 1, ref. L2)], as if $B_{\parallel}$ is amplified there by stretching and shearing (4, 208). The bent jets in the C-shaped head-tail source NGC 1265 are $B_{\parallel}$-dominated even though they are two sided (Table 1, ref. O1). Such fields may be an extreme example of the $B_{\perp\text{-}\parallel}$ configuration resulting from viscous interaction with the ambient medium.

2. Some knots in one-sided jets have $B_{\perp}$-fields although fainter emission near them is $B_{\parallel}$-dominated [e.g. knot A in M87 (172), a knot 50″ from the core of NGC 6251 (183), and knot A2 in Cen A (48)]. These "magnetic anomalies" at bright knots may be due to oblique shocks that accelerate relativistic particles and amplify the component of $\mathbf{B}_j$ parallel to the shock. The fields also become dominated by $B_{\perp}$ components where one-sided $B_{\parallel}$ jets end at bright hot spots, and the physics there may be similar.

The degree of polarization is generally highest at the edges of $B_{\parallel}$-regions, but near the centers of $B_{\perp}$-regions. Two three-dimensional field configurations can fit these polarization distributions: (*a*) tangled field loops confined to a plane perpendicular to the jet axis near the center of the jet (136, 137) but stretched along the axis toward its edges (21, 183), or (*b*) "flux ropes" with helical fields of variable pitch (53) and some random component (183).

## 3.3 *Size, Curvature, and Misalignments*

Jets in weak galaxies (Figure 1) and in powerful core-dominated sources (Figure 5) are generally short ($<10\%$ of all jets in sources with $P^5_{\text{core}} < 10^{22.5}$ W Hz$^{-1}$, and only 13% of those in sources with $P^5_{\text{core}} > 10^{26.5}$ W Hz$^{-1}$, have $d_j > 40$ kpc, but $\sim 50\%$ of those in sources of intermediate powers exceed this length). The jets in core-dominated sources may be shortened by projection effects if the cores are Doppler boosted (Section 6.1.7), but those in weak galaxies are two sided (e.g. Figure 1) and so are probably short intrinsically. Strong jet curvature is also common at the two extremes: C-shaped jets in weak "head-tail" cluster galaxies, and jets in powerful core-dominated sources (Figure 5). The curvature in head-tail sources is probably due to bending by ram pressure (10, 128); that in powerful sources may be due to confinement or to wandering of the central collimator (see Section 6.2.2).

The misalignments between parsec- and kiloparsec-scale jets, summarized in (200), increase with core prominence $f_C$. Several lobe-dominated radio galaxies with kiloparsec-scale jets have cores with one-sided parsec-scale jetlike extensions on the same side as the large jets (Section 6.2.3) and aligning with them to $\leq 10°$ (56, 67, 132, 142, 197–199, 209; Figure 2). In

core-dominated sources, however, parsec- and kiloparsec-scale structures are often misaligned by $>20°$ (57, 69; Figure 4), and in 3C 345 and 3C 418 (Figure 5) by $>90°$. The jets in core-dominated sources bend continuously, with the sharpest curvature occurring closest to the core (58–60, 200, 274; Figure 5). These data are consistent with the short jets in core-dominated sources being close to the line of sight—small bends in jets near the line of sight may project as large apparent misalignments (e.g. 201).

# 4. STRUCTURAL DETAILS

## 4.1 *Collimation, Freedom, and Confinement*

The jets in over a dozen radio galaxies (but in few QSRs) have been resolved transversely well enough to show their lateral expansions directly. They are generally center brightened, supporting the view that jets radiate by dissipation in the energy transport region itself, not in a static cocoon around it. The variation of (deconvolved) synchrotron FWHM $\Phi$ with angle $\Theta$ from the radio core may then track the variation of flow radius $R_j$ with distance $z$ from the nucleus. A steady free jet (whose pressure $p_j \gg p_e$, the sum of all external pressures) would expand with a constant lateral velocity $v_r$ equal to its internal sound speed $c_S$ where it first became free. It would widen at a constant rate $dR_j/dz = v_r/v_j$, unless the flow velocity $v_j$ is slowed by gravity. If $d\Phi/d\Theta = 2(dR_j/dz)$ sec $(i)$, where $i$ is the angle of the jet to the plane of the sky, nonlinearities in $\Phi(\Theta)$ reflect changes in the balance between $p_j$ and $p_e$ with distance $z$. The $\Phi(\Theta)$ data for well-resolved jets show that few are free at all $z$. Their expansion rates are not set once and for all on parsec scales, even though VLBI jets are first collimated on such scales.

4.1.1 WEAK RADIO GALAXIES The first kiloparsec or so of well-resolved jets in weak radio galaxies typically expand with $d\Phi/d\Theta \leq 0.1$ (e.g. 27, 48, 198). Between 1 and 10 kpc, these jets "flare", with $d\Phi/d\Theta$ reaching values of 0.25 to $\sim 0.6$ (e.g. 27, 32, 48, 183). On still larger scales they may recollimate (27, 32, 33, 88, 183, 214, 220, 278). In NGC 315 (278) and NGC 6251 (33, 183), $d\Phi/d\Theta$ oscillates where the jets recollimate; these jets re-expand $>100$ kpc from their cores.

The jet pressure is given by $p_j = p_{jt} + p_{jr} + p_{jm}$, where $p_{jt}$ and $p_{jr}$ are the pressures of the jet's thermal and relativistic particles and $p_{jm}$ is the pressure of its magnetic field $B_j$. The external pressure is $p_e = p_{et} + B_\phi^2/8\pi$, where $p_{et}$ is the thermal pressure and $B_\phi^2/8\pi$ represents confinement by $\mathbf{J} \times \mathbf{B}$ forces of toroidal magnetic fields $B_\phi$ on any current carried by the jet (11, 14, 16, 28, 53, 61, 207, 208). Recollimation requires $p_j \approx p_e$ over many kiloparsecs, but it is unclear which component of $p_e$ dominates. Both halves of two-sided jets tend to recollimate at similar distances from their cores (32, 88, 186, 278).

Those in 2354+47 decollimate as they descend intensity gradients in its soft X-ray halo (49). The synchrotron properties of weak radio galaxy jets set lower limits to $p_j$ ranging from $\sim 10^{-10}$ dyne cm$^{-2}$ in the inner few kiloparsecs to $\sim 10^{-13}$ dyne cm$^{-2}$ $\sim$ 100 kpc from the galactic nuclei. These data suggest, but do not confirm, that weak radio galaxy jets can be collimated solely by $p_{et}$ in hot galactic haloes. Confinement by gas at $\sim$1–3 $\times 10^7$ K [cf. the M87 halo (85)] is (just) compatible with the *Einstein* IPC detections of, or upper limits to, extended soft X-ray sources around several jets, e.g. NGC 315 (278), 3C 66B (152, 168), Cen A (48), and NGC 6251 (183). The contribution of compact nuclear X-ray sources to the IPC data is unclear in some cases, however. *Einstein* and VLA data for M87 (18, 85) show that the minimum $p_j$ in the knots (in this case a few times $10^{-9}$ dyne cm$^{-2}$) exceeds $p_{et}$ at their projected distances in the X-ray halo by at least a factor of 10; only the first few hundred parsecs of this jet can be thermally confined by the X-ray halo, unless the jet is relativistic with $\gamma_j \geq 50$ (18). Nevertheless, its first kiloparsec expands at a constant rate, but the expansion slows beyond knot A; the $B_\phi$ term has been invoked (18) to explain this behavior.

If the longer rapidly expanding segments of these jets are free, the observed $d\Phi/d\Theta \ll 1$ implies that they are supersonic. The data suggest the jets are collimated initially (and become transonic) $<1$ kpc from the nuclei, and that they then escape into regions where $p_e$ drops rapidly. If $p_e$ falls faster than $\sim z^{-2}$, continued confinement of a supersonic jet eventually requires that $v_r > c_S$ (236), so the jet becomes free by "detaching" from $p_e$ at an oblique shock (219). If $p_e$ again falls slower than $z^{-2}$ farther out, as in the X-ray halo of M87 (85, 230), the free jet may be reconfined. Conical shocks would propagate into it from its surface, where it first "feels" the declining gradient of $p_e$, reheating it and possibly (re)accelerating relativistic particles in it (76, and references therein). The shock structure downstream from the reconfinement may be quasi-periodic, leading (*a*) to oscillations in the jet's expansion rate and (*b*) to regularly spaced knots along it (219). These phenomena may have been observed in NGC 315 (278) and particularly in NGC 6251 (33, 183; Figure 2), whose jet is limb brightened near its first reconfinement, consistent with particle acceleration in the conical shocks.

4.1.2 POWERFUL RADIO GALAXIES AND QUASARS The jets in more powerful sources expand more slowly than those in weaker radio galaxies—Table 3 gives the average, minimum, and maximum expansion rates $d\Phi/d\Theta$ for 25 transverse-resolved jets. Several in powerful sources show little systematic expansion, e.g. 3C 33.1 (Table 1, ref. R1), 3C 111 (145), and 3C 219 (184). The small median angle ($<1°$) subtended at the radio cores by "hot spots" in powerful doubles (e.g. 238) supports the trend, if the sizes of the hot spots

indicate (roughly) the diameters of Mach disks where jets terminate (166, 167). The narrower collimation of the jets in stronger sources, coupled with their greater distances, means that their $\Phi(\Theta)$ forms are only crudely known. The data are adequate to show, however, that jets in powerful sources must be either (*a*) free with Mach numbers $\geq 50$, (*b*) confined by much larger external pressures than those in nearby radio galaxies, or (*c*) the approaching sides of relativistic twin jets, whose minimum $p_j$ is overestimated by the conventional calculation due to Doppler boosting (Section 6.1.7); they are all one sided (Section 3.1), so this interpretation is permitted.

Thermal confinement of the parsec-scale jets in several powerful radio galaxies (but not in Cyg A) is compatible with the X-ray data (144), but for several large-scale QSR jets (271) the *Einstein* data rule out pure thermal confinement at $\sim 1$–$3 \times 10^7$ K unless the jets are Doppler boosted. Wardle & Potash (271) argue that freedom is inconsistent with energy and thrust balance (Section 6.1). Eichler (78, 79) discusses balancing $p_{et}$ against the

**Table 3** Expansion data for radio jets

| Jet name | $\log_{10} P^5_{core}$ | $\langle d\Phi/d\Theta \rangle$ | $[d\Phi/d\Theta]_{min}$ | $[d\Phi/d\Theta]_{max}$ |
|---|---|---|---|---|
| 1321+31 SE | 21.77 | 0.30 | $\approx 0$ | 0.4 |
| 1321+31 NW | 21.77 | 0.25 | $<0.07$ | 0.27 |
| 3C 449 N | 22.07 | 0.20 | 0.1 | 0.80 |
| 3C 449 S | 22.07 | 0.20 | 0.1 | 0.45 |
| 3C 129 E | 22.19 | 0.13 | 0.1 | 0.35 |
| Cen A | 22.20 | 0.19 | 0.05 | 0.20 |
| 3C 31 N | 22.45 | 0.30 | 0.08 | 0.38 |
| 3C 31 S | 22.45 | 0.28 | 0.18 | 0.36 |
| 3C 296 (mean) | 22.67 | 0.16 | — | — |
| 0326+39 E | 22.70 | 0.22 | 0.10 | 0.34 |
| 0326+39 W | 22.70 | 0.25 | 0.10 | 0.26 |
| M87 | 22.92 | 0.07 | — | — |
| NGC 315 SE | 23.24 | 0.11 | 0.06 | 0.6 |
| NGC 315 NW | 23.24 | 0.11 | $\approx 0$ | 0.58 |
| 4C T74.17 | 23.26 | 0.12 | — | — |
| Her A W | 23.61 | $<0.1$ | — | — |
| NGC 6251 NW | 23.66 | 0.08 | $\approx 0$ | 0.17 |
| 3C 33.1 | 23.76 | 0.06 | $\approx 0$ | 0.09 |
| Cyg A | 24.12 | 0.03 | — | — |
| 3C 219 | 24.18 | 0.07 | $\approx 0$ | 0.15 |
| 3C 111 | 24.47 | 0.04 | 0.01 | 0.06 |
| 4C 32.69 | 25.15 | 0.06 | — | — |
| 3C 280.1 | 26.21 | 0.05 | — | — |
| 3C 273 | 26.92 | 0.013 | $\approx 0$ | 0.018 |
| 3C 279 | 27.56 | $<0.02$ | — | — |

inertia of low-entropy jets to collimate them. Magnetic confinement is also frequently invoked (11, 14, 16, 53, 191, 207, 208). It requires jet currents of $\sim 10^{17-18}$ A if the fields are near equipartition; the return currents are assumed to lie outside the observed radio emission regions. The QSR jets are $B_{\|}$-dominated (Section 3.2), so the toroidal $B_\phi$ must also be supposed to lie (frustratingly unobserved) outside the main synchrotron-emitting regions.

4.1.3 COCOONS The study of jet collimation is complicated by sources such as M84 (Figure 1), 3C 341 (Figure 6), 1321+31 (88), 4C 32.69 (75), and 2354+47 (49) with faint emission "cocoons" around brighter jets. The collimation properties of cocoons may differ radically from those of their jets, e.g. that in M84 (Figure 1) expands much faster than the jets at $\Theta > 5''$. At what level of brightness (if any) in such sources does the synchrotron expansion rate $d\Phi/d\Theta$ indicate streamline shapes in an underlying flow? The minimum cocoon pressures are only $\sim 0.1\ p_j$ (if the jets are unbeamed), so thermal confinement of the jets should crush the cocoons (75). The relationship of cocoons to the brighter structure—whether they are faint "outer jets," static sheaths, or backflows such as those in simulations of thermal matter flows in jets (166, 167)—is unclear. Polarimetry of the cocoons may test whether they contain the $B_\phi$ required for magnetic confinement of the jets, by detecting radial changes in $\mathbf{B}_a$ or transverse rotation measure gradients (183).

## 4.2 *Radio Spectra*

About 40% of jets have spectra between $\nu^{-0.6}$ and $\nu^{-0.7}$ near 1.4 GHz, and $\geq 90\%$ have spectra between $\nu^{-0.5}$ and $\nu^{-0.9}$. Spectral gradients along most jets are small, but where they have been detected the spectra steepen away from the cores (48, 54, 70, 75, 245), consistent with synchrotron depletion of the higher-energy electrons in the outer jets (277).

## 4.3 *Intensity Evolution*

Both the magnetic field strengths and the relativistic particle energies will decrease along an expanding laminar jet, with no magnetic flux amplification or particle reacceleration. If (*a*) magnetic flux is conserved and (*b*) the radiating particles do work, as a jet with the typical $\nu^{-0.65}$ spectrum (Section 4.2) both expands laterally and responds to variations in its flow velocity $v_j$, then the jet's central brightness $I_\nu$ will vary as $R_j^{-5.2} v_j^{-1.4}$ in $B_{\|}$-dominated regions, or $R_j^{-3.5} v_j^{-3.1}$ in $B_\perp$-dominated regions (88, 183). Note that neither $B_{\|}$ varying as $R_j^{-2}$ nor $B_\perp$ as $R_j^{-1} v_j^{-1}$ to conserve magnetic flux are compatible with equipartition of energy between radiating particles and $B_j$ in a confined jet if the particles do work and are not reaccelerated;

equipartition requires $B_j$ to vary as $R_j^{-4/3}v_j^{-0.3}$ and $I_\nu$ to decline as $R_j^{-4.1}v_j^{-1.9}$ for a $\nu^{-0.65}$ spectrum. Actual variations of $I_\nu$ with jet FWHM $\Phi$ (assumed proportional to $R_j$) are often much slower than these "adiabats" over large regions of the jets (27, 118, 183, 278). Near the core, $I_\nu$ often increases with $\Phi$—the jets "turn on" following regions of diminished emission, or "gaps" (19, 29, 186, 277; Figures 1, 3, 6). The "turn-on" is often followed by regimes many kiloparsecs long in which $I_\nu$ declines as $\sim\Phi^{-x}$, with $x = 1.2$–$1.6$; the value of $x$ reaches $\sim 4$ in the outer regions of some jets (33, 117, 183, 278), but in NGC 6251 the "adiabatic" decline $\geq 100$ kpc (200″) from the core is repeatedly interrupted by the "turning on" of bright knots (see Figure 2 and 183).

It is likely that some of the bulk kinetic energy of the jets (which is not lost by adiabatic expansion) is converted to magnetic flux and relativistic particles through dissipative interactions with the surrounding ISM. Indeed, if $B_j$ is near equipartition on kiloparsec scales, $B_\parallel$ must be amplified locally (instead of falling as $R_j^{-2}$) or else long $B_\parallel$-dominated jets would have unreasonably high fields on parsec scales. Models for "reheating" of jets include shock formation (24, 66, 167, 219) and various mechanisms following the development of large-scale vortical turbulence (8, 13, 15, 17, 73, 82, 94, 112, 118) from the growth of instabilities at the jet surface. Some models based on large-scale turbulence link the synchrotron emissivity directly to the turbulent power, and hence to the jet spreading rate as $(d\Phi/d\Theta)^n$ with $1.5 \leq n \leq 3$ (17, 82, 118). They can thereby explain why the rapidly expanding jets in weak sources (Table 3) are so conspicuous, and why a jet's most rapidly expanding segments are often those of its most "subadiabatic" intensity evolution (118, 183). Initially laminar jets may also propagate far from their sources before becoming turbulent; rapid fading in the laminar ("adiabatic") regime (as in parsec-scale VLBI jets; Figure 4) can be followed by "turning on" of a large-scale jet in the same direction once turbulence becomes well developed. This may explain the "gap" phenomenon (8, 13, 17, 118, 129). Velocity variations may also keep jets bright in two distinct ways. Fluctuations in $v_j$ at the core can produce strong shocks that locally enhance the synchrotron emissivity (206). Entrainment of surrounding material will decrease $v_j$ along a jet—the resulting axial compression may partly compensate the effects of lateral expansion, particularly where $B_\perp$ dominates (88, 183).

Detailed understanding of what keeps large-scale jets lit up requires self-consistent modeling of their collimation, intensity evolution, and magnetic field configurations. Abrupt changes in $\mathbf{B}_a$ from $B_\parallel$ to $B_\perp$ at bright knots (Section 3.2) may indicate particle acceleration at oblique shocks, particularly if the knots have their sharpest brightness gradients on their coreward sides, as in M87 (18, 54) and NGC 6251 (183). The degrees of

linear polarization in, and the depths of, $B_{\parallel}$ edges on $B_{\perp}$-dominated jets may indicate the extent of viscous interactions with the surrounding ISM. The observations provide copious constraints for the models: jet expansion rates, "turn-on" heights, transverse intensity profiles, field orderliness and orientation, as well as the $I_\nu(\Phi)$ evolution. Models of jet propagation are not yet sufficiently versatile to confront the data at all of these points self-consistently, however.

# 5. RADIO JETS AT OTHER WAVELENGTHS

## 5.1 *Optical and Infrared Wavelengths*

5.1 CONTINUUM Optical continuum emission coincides with bright knots in the radio jets of 3C 31 and 3C 66B (52), M87 (249, and references therein), 3C 273 (2, 141, and references therein), 3C 277.3 (159), and possibly Cen A (34). The spectral index between 4500 Å and 5 GHz is generally within 0.1 of 0.7 (52). The M87 knots all have essentially the same connected optical-infrared-radio spectra, with slopes in the radio, infrared, and optical of $\sim$0.6, 0.8, and 1.7, respectively; the latter spectral break occurs near 6000 Å in every bright knot (150, 165, 237, 244). In 3C 273 the radio jet brightens toward its tip (64, 181) but the optical jet is more uniformly bright, except for knots at each of its bends (141), so the spectrum above 5 GHz steepens with distance from the QSO (cf. Section 4.2).

The optical continuum is up to 20% linearly polarized in M87 (226, and references therein) and $\sim$14% linearly polarized in 3C 277.3 (158, 159). This polarization, the positional coincidence with the radio knots, and the connected optical-radio spectrum in M87 are evidence that the optical continuum is synchrotron radiation from the same regions as the radio jets. The overall linear polarization of the optical jet in 3C 273 is only $3.7 \pm 4.1\%$ (226), whereas the radio jet is $\sim$12% polarized at both 1.4 and 5 GHz at 2″ resolution (Table 1, ref. P2). The radio **E** vectors in the "head" and "tail" of this jet are nearly perpendicular, however, so high-resolution optical polarimetry is needed to test whether the optical emission is synchrotron radiation there also. If $\mathbf{B}_j$ is near equipartition in these jets, the electrons radiating at optical wavelengths are several synchrotron lifetimes from the radio cores. The distribution of optical emission marks the sites of relativistic electron reacceleration, or possibly of pitch angle scattering (239, 240), better than the radio data because of the much longer synchrotron lifetimes of the radio electrons. Studies of optical jets with the *Space Telescope* will show how discrete, or continuous, the reacceleration regimes are.

5.1.2 EMISSION LINES Data on emission lines from the vicinity of radio jets are reviewed in (158) and (260). The line-emitting regions generally lie

beside or beyond the jets, particularly on the outer edges of bends, and are often brightest near, but not at, knots or hot spots. The spectra are not those of normal H II regions, but instead resemble those of Seyfert 2 nuclei. Typical densities are $\sim 10^2$ to $10^3$ cm$^{-3}$ and temperatures $\sim$20,000 K, leading to pressures near the lower limits to $p_j$ in adjacent radio features. Typical bulk velocities are a few hundred kilometers per second, and line widths are 300–500 km s$^{-1}$. In Cen A, some emission-line filaments beyond the jet have internal differential velocities up to 800 km s$^{-1}$ (106); they cannot stay intact long enough to have been convected out from the nucleus. The line strengths suggest photoionization by a power-law continuum, and possibly also shock heating, with different mixtures of excitation mechanisms in different sources. The occurrence of this extranuclear line emission at the edges of radio features, and the increase of line widths toward them (116), suggest interaction between jets and the ambient ISM. The line-emitting gas may be clouds in normal galactic rotation that have encountered jets, becoming heated, ionized, and accelerated by them (26, 73, 74, 116, 158, 159, 282). The uncertain dynamics of the emission-line gas preclude using its bulk velocities to infer jet velocities directly, as suggested in (159).

A continuum and emission-line feature in DA 240 has been reported as an "optical jet" blueshifted relative to the galactic nucleus by 3400 km s$^{-1}$ (40, 41). This has been invoked (41, 246) as direct evidence that $v_j = 3400$ km s$^{-1}$ in DA 240, but the feature is not a radio jet and may be a confusing spiral galaxy (261).

## 5.2 *X-Ray Wavelengths*

Three radio jets are known to be X-ray sources—M87 (230), Cen A (228), and 3C 273 (276). [See (90) for a review and further references.] The region near the M87 jet has a luminosity of $\sim 10^{41}$ erg s$^{-1}$ in the *Einstein* HRI band. Individual knots are not resolved, but this integrated X-ray luminosity is consistent with extrapolating the steep spectrum of the knots above 6000 Å to the X-ray regime. If the synchrotron interpretation favored in (230) is correct, electrons with $\gamma \approx 10^{7.3}$ are required to produce the observed X-rays in the equipartition magnetic field of the knots; this provides a severe test for particle acceleration models. The radiative lifetimes of such electrons would be $\leq$200 yr, comparable to the light crossing time in the knots, but much less than the light travel time to the knots from the nucleus of M87. The X-ray and radio structures of the jet in Cen A are also very similar (48), suggesting that this is also synchrotron emission, though the case is not as strong as for M87 (90). The detection of the X-ray jet in 3C 273 depends heavily on deconvolution of the point-source response from the data, so it has not yet been analyzed in detail.

# 6. JET LAG-MISSING PHYSICS

## 6.1 *Velocity Estimates*

Without direct velocity indicators such as emission lines from material in the jet flows, estimates of the average flow velocities $v_j$ are indirect and sensitive to the initial assumptions. Most methods assume jet properties to be stationary in time and estimate $v_j$ from observables using one or more of the following arguments.

6.1.1 ENERGY FLUX If synchrotron losses from a lobe of luminosity $L_{lobe}$ are continuously replenished by the energy influx from a jet at an efficiency $\varepsilon$, the energy flux supplied to the lobe must be $L_j = L_{lobe}/\varepsilon$. The flux $L_j$ is related to other jet parameters by

$$L_j = A_j \rho_j v_j^3 \gamma_j^2 \left[ \frac{\gamma_j}{\gamma_j + 1} + \frac{h_j}{\rho_j v_j^2} \right],$$

where $A_j$, $v_j$, $\rho_j$, $\gamma_j$, and $h_j$ are the cross-sectional area, flow velocity, density, Lorentz factor, and enthalpy per unit rest mass of the jet at some point along it, respectively. (The transverse structure of the jet is usually ignored when estimating $v_j$.)

6.1.2 MOMENTUM FLUX For jets which terminate at hot spots, the thrust $T_{j/h}$ in the rest frame of the hot spot must balance $p_h A_h$, where $p_h$ and $A_h$ are the minimum pressure and cross-sectional area of the hot spot estimated from its synchrotron parameters. The thrust $T_j = A_j \rho_j v_j^2 \gamma_j^2$ in the galaxy or QSR frame can be calculated from this by assuming the dynamics of the interaction between the hot spot and the ambient density $\rho_e$ to relate $v_j$ to the velocity $v_h$ of advance of the hot spot. Estimates for $T_j$ can also be made for C-shaped jets in "head-tail" sources if these jets are bent by the ram pressure of an intergalactic density $\rho_e$ through which their parent galaxy moves at velocity $v_g$ (10, 128). If the radius of curvature of the C-structure is $R_c$ and the scale over which the ram pressure is transmitted to the jet is $H$, momentum balance requires that $T_j = \rho_e v_g^2 A_j R_c / H$. The parameter $H$ is the radius $R_j$ of the jet in the "naked" jet-bending model of (10), but it is a scale associated with the ISM of the parent galaxy in the "shielded" model of (128).

6.1.3 MASS FLUX The mass flux $dm/dt = A_j \rho_j v_j \gamma_j$ down the jet must meet either reasonable constraints on the rate of ejection from the "central engine" or constraints from depolarization data on the total mass injected into the lobes over the lifetime of the source. (The latter constraints are generally less stringent, but they could be tightened by high-resolution polarimetry of lobes at frequencies below 1 GHz.)

6.1.4 JET EXPANSION The Mach number $M_j$ of a free jet where it detached from its confinement (Section 4.1) can be estimated from its synchrotron expansion rate via $d\Phi/d\Theta = (2/M_j)$ sec $(i)$, where $i$ is the (assumed) angle between the jet axis and the plane of the sky. Then $v_j = M_j\sqrt{\Gamma p_j/\rho_j}$, where $\Gamma$ is the ratio of principal specific heats in the jet, and a lower limit to $p_j$ is obtained from the synchrotron parameters. If the jet is actually confined, $M_j$ is overestimated. If the weak radio galaxy jets are alternately free and confined (Section 4.1.1), $M_j$ is best indicated by the rapid expansions at $z \approx 1$–10 kpc, which imply that $M_j \approx 10$ there.

6.1.5 ELIMINATING THE JET DENSITY Usage of the techniques of Sections 6.1.1–6.1.4 alone requires estimates of $\rho_j$, generally from centimeter-wavelength Faraday depolarization data that are hard to obtain and to interpret (87). High signal-to-noise is needed to reduce Ricean bias in the polarized signal (183, 270). The configuration of $\mathbf{B}_j$ is unclear (Section 3.2), particularly the scale distribution of its reversals, which may "hide" thermal gas. Some jets are surrounded by emission-line filaments (Section 5.1.2) and magnetoionic media with clumping scales of $\sim$1–5 kpc (33, 183; Table 1, ref. L2). Differential Faraday rotation across the radio beam by such media may decouple the observed depolarization from $\rho_j$, so even setting limits to $\rho_j$ from low-resolution depolarization data without mapping the rotation measure gradients is hazardous, especially at low frequencies. The methods in Section 6.1.1–6.1.4 all permit $v_j \to c$ if $\rho_j \to 0$, but Table 4 shows how $v_j$ can be constrained using combinations of these methods to eliminate $\rho_j$ for "cold" ($h_j \ll \rho_j v_j^2$) jets. As $h_j/\rho_j v_j^2 = \Gamma/M_j^2(\Gamma-1)$ from the gas laws and Section 6.1.4, this is a good assumption for jets with $M_j \geq 4$. These combinations also eliminate $A_j$, bypassing the (uncertain) relationship between the jet's synchrotron width $\Phi$ and its flow radius $R_j$. They normally yield velocities in the range $1000 < v_j < 30{,}000$ km s$^{-1}$ unless low efficiencies $\varepsilon$ or high mass fluxes $dm/dt$ are assumed.

**Table 4** Parameter combinations for cold jets

| Combination | $v_j \ll c$ | $\gamma_j \gg 1$ |
|---|---|---|
| $\left[\frac{L_j}{cT_j}\right] = \sqrt{\frac{\gamma_j-1}{\gamma_j+1}}$ | $\frac{\beta_j}{2}$ | 1 |
| $\left[\frac{L_j}{c^2(dm/dt)}\right] = \gamma_j - 1$ | $\frac{\beta_j^2}{2}$ | $\gamma_j$ |
| $\left[\frac{T_j}{c(dm/dt)}\right] = \sqrt{\gamma_j^2-1}$ | $\beta_j$ | $\gamma_j$ |

6.1.6 SUPERLUMINAL MOTION A simple model for the observed proper motions of knots in compact sources (57) is that apparent "superluminal" motion at $\beta_{app} = v_{app}/c > 1$ arises for features in the approaching side of a high-$\gamma_j$ jet at a large angle $i$ to the plane of the sky, whereupon $v_j = v_{app}/[\beta_{app} \sin(i) + \cos(i)]$.

6.1.7 DOPPLER BOOSTING With the above notation, $v_j$ is related to the ratio of intensities $\mathcal{S}_{app}$ of the approaching and receding sides of an intrinsically symmetric ($\mathcal{S} = 1$) jet as $v_j \sin(i) = c[\mathcal{S}_{app}^{\delta} - 1]/[\mathcal{S}_{app}^{\delta} + 1]$, where $\delta = 1/(2+\alpha)$ for a continuous jet with a $\nu^{-\alpha}$ spectrum (23). Assuming $\mathcal{S}_{app}$ to be due entirely to Doppler boosting therefore constrains $\beta_j \sin(i)$. Note that with the typical value $\alpha = 0.65$ (Section 4.2), $\mathcal{S}_{app}$ varies as $\gamma_j^{5.3}$ if the line of sight is $< 1/\gamma_j$ radians from the jet axis; also, note that a jet can be "one sided" as in Section 3.1 ($\mathcal{S}_{app} > 4:1$) if $\beta_j \sin(i) > 0.26$, which at $i = 30°$ (the median value for randomly oriented sources) requires only that $\beta_j > 0.52$.

6.1.8 JET WIGGLING Many jets wiggle around their mean direction (e.g. 29, 172, 183, 214, 220, 262, 263). Mechanisms for periodic lateral deflections $\Delta$ as a function of angle $\Theta$ from the core [reviewed in (252)] include (*a*) orbital motion of the primary collimator around a companion mass in the parent nucleus (9, 151) or a nearby member of the same group or cluster (22, 263); (*b*) precession of the primary collimator or of a larger-scale recollimating atmosphere due to interaction with another body (9, 104, 123, 143, 205, 284); and (*c*) growth of helical Kelvin-Helmholtz instabilities at the boundary of a confined jet (Section 6.4). Pure orbital motion leads to C-symmetry between the two sides of a jet, with fixed wiggle amplitude $\Delta$ and a period $\tau_o$. Pure precession of the source of a free nonrelativistic jet leads to S-symmetry, linear growth of $\Delta$ with $\Theta$, and a period $\tau_p$. The analogue for relativistic jets is more complicated as the S-symmetry is broken by light travel time effects, which might themselves indicate $v_j$ if other distortions were absent (63, 104, 143). Helical surface instabilities on a confined expanding jet make wiggles whose amplitudes $\Delta$ and wavelengths $\lambda_i$ both grow with $\Theta$; linear theory has been used to estimate the most rapidly growing wavelength $\lambda_i$ as a function of jet radius $R_j$, Mach number $M_j$, and density contrast $\rho_j/\rho_e$ (Section 6.4).

Attempts to constrain $v_j$ from jet-wiggling data "match" an observed pattern $\Delta(\Theta)$ to one of these pure forms to find a characteristic wavelength $\lambda_O$ and a self-consistent estimate of the characteristic period $\tau_o$ or $\tau_p$. Then, $v_j$ or $M_j$ is derived from one of the following: $v_j = \lambda_O/\tau_o$, $v_j = \lambda_O/\tau_p$, or $\lambda_O \approx \lambda_i = R_j F_1(M_j) F_2(\rho_j/\rho_e)$, where the functions $F_1$ and $F_2$ are provided by (linear) instability theory. These methods are fraught with uncertainties. Well-studied jets rarely match simple orbital or ballistic precessional

shapes convincingly (22, 104, 105, 257), so additional poorly constrained parameters (e.g. multiple or eccentric orbits, variation of precession cone angle with time) are invoked. Even goodness of fit to a simple C- or S-shape does not guarantee uniqueness of the model (63, 122). Bending and buoyancy effects (e.g. 119, 235, 283) may also be present and—unless the jet is denser than the ambient medium—lateral motions may excite surface instabilities, whose growth also alters the shape of the jet (12). Linear instability theory may be inadequate to describe any mode that grows sufficiently to become detectable on radio maps.

## 6.2 *The Velocity Dilemma*

The above methods give velocities ranging from $v_j \approx 1000$ km s$^{-1}$ in C-shaped jets in head-tail sources (using Section 6.1.2) to $\approx c$ (using Section 6.1.6 to interpret one sidedness or Section 6.1.7 to interpret superluminal motion). This uncertainty in $v_j$ seriously obstructs progress in elucidating the physics of radio jets.

6.2.1 ARGUMENTS FOR $v_j \approx c$ ON PARSEC SCALES Five arguments favor $v_j \approx c$ on parsec scales in some sources:

1. The superluminal separations of knots in VLBI "core-jet" structures can be explained if $\gamma_j \approx 2.5$–10 (for $H_0 = 100$) and these structures are within $\sim 1/\gamma_j$ radians of the line of sight (Section 6.1.6).
2. The same parameters entail Doppler boosting (Section 6.1.7), which accounts for the one sidedness of these VLBI core-jets.
3. Similar assumptions (but with higher values of $\gamma_j$) may explain the high brightness temperatures implied by the rapid low-frequency variability of some compact radio sources (89, and references therein).
4. The same assumptions explain the low Compton X-ray fluxes from compact radio sources (e.g. 155).
5. The small angles to the line of sight ($i \approx 90°$) required by this interpretation of the properties of strong compact cores are consistent with the large apparent bending of the jets in core-dominated sources (Section 3.3).

There is little evidence against $v_j \approx c$ on parsec scales: 3C 147 has a complex, *two*-sided parsec-scale structure (194), but two sidedness may be ascribed to bending a one-sided jet across the line of sight, in a suitably small number of cases, without endangering the relativistic-jet picture of compact sources.

6.2.2 ARGUMENTS AGAINST $v_j \approx c$ ON KILOPARSEC SCALES The sensitivity of Doppler boosting (Section 6.1.7) to $v_j \sin(i)$ argues against $v_j \approx c$ in the C-shaped jets in "narrow head-tail" sources. If these are indeed swept back by ram pressure of the intergalactic medium (Section 6.1.2), $\mathbf{v}_j$ changes

direction along them by as much as 90° (e.g. 171, 214, 257). If $v_j \approx c$, they would (*a*) have large side-to-side asymmetries and (*b*) brighten or fade dramatically as they bend, in conflict with observation (265). The orientations of dust lanes in some weak radio galaxies also suggest that brightness asymmetry at the bases of their two-sided jets (Section 3.1) is unlikely to be due to Doppler favoritism. The jets are generally $>70°$ from the dust lanes in projection (134 and Table 1, ref. L1), so they should generally be nearly perpendicular to them in three dimensions. The orientation of the dust lane (266) in M84 thereby suggests that the northern jet, which is the brighter and has the one-sided base (Figure 1), is either receding or very close to the plane of the sky (if it is an outflow). Both this constraint and the fact that it becomes two sided without bending argue that its greater brightness is due to greater power output or greater dissipation on its side of the nucleus, rather than to Doppler boosting. R. A. Laing (personal communication) finds similar results in NGC 3665 and for the possible jet in NGC 612, although in Cen A the peculiar velocities of the optical filaments (Section 5.1.2) argue that the bright radio jet is approaching.

This evidence against $v_j \approx c$ in sources with $P_{tot}^{1.4} < 10^{25}$ W Hz$^{-1}$ (FR I structures) leaves open the possibility that $v_j$ increases with $P_{tot}$, so that the long one-sided jets in powerful sources might be Doppler-boosted flows with $\gamma_j \gg 1$. Some bent one-sided jets have smooth brightness variations [e.g. 1150+497 (Figure 3), 4C 32.69 (191)], which are inconsistent with changing Doppler boosts in high-$\gamma_j$ jets if they bend because they are confined. Such jets could be ballistic, however, with their shapes arising from wobble (precession?) of the primary collimator; $\mathbf{v}_j$ would then not follow the bends, but the wiggle pattern would move radially as a whole. Changes in $v_j \sin(i)$ and in the Doppler boosting (Section 6.1.7) may then be small. We must know whether or not such jets are confined (Section 4.1), and if so where, to decide whether their brightness distributions argue against $v_j \approx c$. Doppler boosting models for long one-sided jets also require large angles $i$, so boosted one-sided jets would be significantly longer in three dimensions than they appear in projection. It is unclear whether this seriously conflicts with $v_j \approx c$ in these jets, as the existing statistics of QSR source sizes come from samples containing significant numbers of one-sided jets (Section 2.2). Maps with greater dynamic range are needed to assess the degree of one sidedness of these jets (we do not know by how much $\mathcal{S} > 4$ in most cases), as the average deprojection increases with the average asymmetry.

6.2.3 ARGUMENTS FOR $v_j \approx c$ ON KILOPARSEC SCALES Table 1 lists 22 sources with VLBI jets or elongations. Of these, five exhibit superluminal expansion—3C 120, 3C 179, 3C 273, 3C 279, 3C 345 (57). In all five, the

kiloparsec- and parsec-scale jets start on the same side of the core, as in Figure 4 (see references in Table 1). Sixteen others have VLBI elongations and kiloparsec-scale jets, but their proper motions on parsec scales are unknown. In 11 of these (NGC 315, 3C 78, 3C 84, 0957+56, 3C 111, M87, Cen A, NGC 6251, 3C 371, 3C 405, and 3C 418), the larger-scale jet starts on the same side as the small, e.g. Figures 2 and 5. Of the remaining five, two (3C 147 and 3C 236) have two-sided small-scale structure, two (M84 and 3C 454.3) do not have closure-phase VLBI maps, and 3C 309.1 has complex structure. The correlation between small- and large-scale sidedness argues that one sidedness has the same cause on both scales. It supports the idea that $v_j$ can be high enough on kiloparsec scales for Doppler favoritism to be important, if one is convinced by the case for $\gamma_j \gg 1$ on parsec scales (Section 6.2.1). This case is strongest for the five superluminal sources, but it is not yet impregnable. Since there are no known coreless large-scale jets, either both the cores and the jets are Doppler boosted or the luminosities of intrinsically one-sided jets are coupled to those of the cores; the reason for such coupling over such a wide range of linear scales is unclear if the sidedness is due to asymmetric dissipation. If the kiloparsec-scale sidedness is intrinsic (124, 213, 218, 273, 280), these data require a switching time-scale $\tau > d_j/v_j$ and an alternative model for superluminal expansions. The constraint $\tau > d_j/v_j$ is often hard to reconcile with $\tau$ being less than the synchrotron lifetimes in the hot spots (e.g. 113, 265). On balance, the correlation between parsec and kiloparsec sidedness favors $\gamma_{core} \approx \gamma_j \geq 1$ in powerful sources.

Other (weaker) arguments for $v_j \approx c$ on kpc scales are the following:

1. Relativistic jets need less confinement, since Doppler boosting and projection effects at large angles to the plane of the sky mean that the standard synchrotron calculation may overestimate $p_j$.
2. It is difficult to brake a jet by entrainment between the parsec and kiloparsec scales without converting much of its energy into heat, unless $M_j$ is low (222). Losing $\sim c/v_j$ times the total power of a strong extended radio source by dissipation as "waste heat" near its nucleus is a daunting prospect for source models if $v_j \ll c$.

## 6.3 *Jet/Hot-Spot Symmetries and the Sidedness Dilemma*

The symmetries of the regions where powerful jets end may also offer clues to the reasons for their one sidedness (215). If it is always due to Doppler favoritism, the jetted and unjetted lobes should look similar—unless high-$\gamma_j$ jets push the hot spots out at $v_h \approx c$, in which case the brighter jet should appear to feed the brighter and more distant hot spot if the two sides of the source have the same history (146). (In the extreme case of a "young" high-$\gamma_j$ source, radiation from the receding side may also not yet have reached us.)

In 34 of the 46 FR II sources in Table 1 with one-sided jets, one lobe has a significantly brighter hot spot than the other on the highest resolution map available. Seventeen of the 34 have $f_C = S^5_{core}/S^{1.4}_{tot} > 0.05$; the brighter jet points to the brighter hot spot in 16 of these. Unless the jets are "young", either the brighter jet has a higher thrust or the jets and the hot spots in these sources are both Doppler boosted. In the 17 cases with $f_C < 0.05$, the brighter jet points to the brighter hot spot in ten and to the weaker in seven. This is consistent with one sidedness due either to differential dissipation or to Doppler boosting. There is no trend in either group for the jetted hot spot to be more distant, so if boosting is important the hot-spot separations must not reflect travel time differences from simultaneous ejecta. They might instead be determined by the history of the source, e.g. by a wandering or intermittent jet illuminating different parts of a lobe at different times. These trends imply that either (*a*) jet one sidedness has different causes in FR II sources with different $f_C$, or (*b*) the jets, but not the hot spots, are boosted in sources with $f_C < 0.05$, while both are boosted if the core is strong. The relative brightnesses of hot spots are sensitive to linear resolution, however, so the trends must be checked with more uniform data.

## 6.4 *Stability*

Jets are surprisingly stable. They can extend for hundreds of kiloparsecs or bend through $\geq 90°$ (in C-shaped "head-tails") without disruption. Early analyses of the stability of confined cylindrical jets to helical, fluting, and pinching perturbations analogous to the Kelvin-Helmholtz instabilities of a vortex sheet (15, 92, 93, 95, 110, 195) suggested that jets are generally unstable to modes with wavelengths of a few jet radii. The growth rates are less for $M_j > 1$ and for $v_j \approx c$, but the stability of observed jets forces re-examination of simplifying assumptions made in these analyses. The stabilizing influence of a surface shear layer on modes with wavelengths less than its scale depth was examined in (92) and (196), and that of jet expansion on long-wavelength modes in (111). Within a thermally confined jet, $B_{\|}$ may stabilize long-wavelength pinching modes (12, 92, 195). The firehose instability can be inhibited by sizable $B_j$ and by linking the inertia of a plasma cocoon around the jet to $B_j$ (12). The stability of magnetically confined jets has yet to be studied thoroughly, although first steps have been taken (12, 16, 61). Progress here is hampered by ignorance of basic MHD parameters in jets: we know little about ion or electron temperatures, field strengths, particle densities, and sound or Alfvén speeds, independent of the assumption of equipartition. Currently favored models of jet production from rotating disks or tori near supermassive objects (e.g. 251) may produce flows with net helicity. The influence of such helicity on

jet stability merits attention, as helicity can lead to efficient generation of large-scale $\mathbf{B}_j$ by turbulent amplification of small seed fields (72).

Instabilities in real jets may grow algebraically, rather than exponentially. Exponential growth can be stopped in many ways—shock formation when the perturbation velocities become supersonic, shifting of the modes to longer wavelengths as their amplitudes grow, or saturation of the instabilities by in situ particle acceleration (15, 93, 94). Nondestructive instabilities might dominate the observed shapes and relative brightnesses of radio jets and lobes (15, 112, 286): algebraic growth of short-wavelength instabilities may help to keep jets bright (Section 4.3), long-wavelength helical modes to explain jet wiggling (Section 6.1.8), and pinching modes to form knots (Sections 4.1.4 and 4.3). Instability growth may also determine overall source sizes. MHD stability analyses including jet expansion, velocity and density gradients, and realistic $\mathbf{B}_j$ configurations and velocity profiles are needed; the analytical difficulties are great, and numerical simulations that do not legislate axisymmetry may be required.

## 6.5 *Unified Models*

"Unified" models seek to relate differences between sources with weak and powerful radio cores solely to differences in viewing angle. If the arguments in Section 6.2.1 indeed support $\gamma_j \gg 1$ and $i \approx 90°$ in the jets of core-dominated sources, a randomly oriented sample should contain $\sim 2\gamma_j^2$ unboosted sources for every boosted one if the jets have narrow cone angles. For $\langle \gamma_j \rangle \approx 5$ (169), core-dominated sources would number only a few percent of their parent population in the plane of the sky, which may therefore be a well-known class of object. Proposed parent populations for the core-dominated QSRs are radio-quiet QSOs (223) and QSRs with lobe-dominated extended radio sources (23, 169). The latter proposal is not encouraged by the fact that the lobe-dominated sources have weaker [FeII] emission and broader lines than core-dominated sources (242, 281). It is hard to see how such differences in the line strengths could be produced by the small aspect differences ($\Delta i \approx 1/\gamma_j$ radians) over which the Doppler-boosting factor varies markedly (115). Although the flux density distribution of strong radio sources in optically selected QSO samples conflicts with the unified models (131, and references therein), VLA studies of the Schmidt-Green QSO sample to a limiting flux density of 250 $\mu$Jy at 6 cm are consistent with them over most of the flux density range. The "excess" of strong sources may be due to a separate population of extended sources, most of whose emission is presumably unbeamed (K. Kellermann et al., in preparation). As the emission lines cannot be beamed, models that beam the optical continuum luminosities of core-dominated QSRs predict the existence of emission-line QSOs without nonthermal continua; these have not been detected.

About half of all core-dominated sources have detectable kiloparsec-scale secondary structure, which is generally one sided, as in Figure 5 (182, 185, 274). If the parent population is to be "radio quiet" (223) or to have normal two-sided lobes (169), both "unified models" must assert that most of this one-sided secondary structure is also boosted. The parent population of most core-dominated sources must then be a class of numerous weak extended radio sources with at least mildly relativistic kiloparsec-scale jets and relatively strong Fe lines.

## 6.6 *A Broader Unified Model*

As about half of all radio galaxies and nearly all QSRs have detectable radio cores (131, and references therein), there must be a mixture of boosted and unboosted contributions to the core emission. Furthermore, some kiloparsec-scale jets emerging from weak cores must have nonrelativistic velocities and intrinsic emission asymmetries (Section 6.2.1), while some jets emerging from powerful cores may be relativistic (Section 6.2.3). It may be that $\gamma_{\rm core} \geq \gamma_{\rm j} > \gamma_{\rm h}$ in all sources, while all three tend to increase with the actual source power (measured by the luminosity of the most extended radio features). The correlations between $P_{\rm core}$ and $f_{\rm C}$, the occurrence rates of jets (Section 2.3), their sidedness (Section 3.1), their magnetic field configuration (Section 3.2), and the large-scale source structure (FR class) might be assimilated in a broader unified model as follows.

The kiloparsec-scale jets in most weak sources have $v_{\rm j} \ll c$, and so appear two sided, with minor asymmetries that are either intrinsic or the result of asymmetric internal dissipation of flow kinetic energy to synchrotron radiation. They expand rapidly, so $B_{\perp}$ dominates over $B_{\parallel}$ except at their bases. They have low thrusts and so are readily bent, sometimes maintaining $B_{\parallel}$ layers at their edges by shearing or stretching as they bend. Low Mach numbers allow them to become turbulent, to entrain material and thus to decelerate [all effects that keep them well lit up (Section 4.3)], and to terminate gently without forming hot spots. These characteristics lead to FR I morphology (Figure 1). Weak sources with $\gamma_{\rm j} = \gamma_{\rm h} \approx 1$ but $\gamma_{\rm core} \gg 1$ would be strongly core dominated if oriented near the line of sight; their extended low-brightness FR I structure would be detected only on maps with high dynamic range. Such sources could be BL Lac objects with very weak large-scale structure (23, 37, 254). There cannot, however, be large numbers of sources with $\gamma_{\rm core} \gg \gamma_{\rm j}$, or else we would see many "coreless jets."

The kiloparsec-scale jets in more powerful sources may have higher $v_{\rm j}$. They may also have higher Mach numbers, leading to narrower cone angles where they are free and to prominent hot spots where they end. They may be more stable, less turbulent, and thus dimmer relative to their lobes, leading to FR II morphology. Higher $v_{\rm j}$ may lead, however, to deeper

boundary layers with the intergalactic medium, in which $B_{\|}$ is maintained by shearing (129, 208). The combination of such shearing and good collimation could make the jets that do stay lit up appear $B_{\|}$-dominated (Section 3.2) at low transverse resolution. If $v_j \rightarrow c$ in the more powerful sources, Doppler boosting may contribute to correlations between jet detectability, $f_C$, and jet/hot-spot symmetries (Section 6.3). The jets and some core emission in powerful sources near the plane of the sky would be beamed away from us, producing "jetless" FR II sources with weak cores, as in the distant 3CR[2] radio galaxies (Section 2.2). Similar sources turned toward us would have strong cores and one-sided jets, as in the extended 3CR[2] QSRs. The $\sim$40 to 50% detection rate of jets in 3CR[2] QSRs requires, however, that only mild boosting ($\gamma_j \leq 2$) is usually involved, and the lack of "coreless jets" again implies that $\gamma_{core} \approx \gamma_j$ in general. Intrinsic asymmetries may therefore still be significant in the powerful sources. There are weak relationships between $f_C$ and projected linear size, misalignments, and lobe separations among extended QSRs (130); these relationships are consistent with some core boosting in these sources.

Such "unified models" of extragalactic radio sources may ultimately be judged by whether or not the optical and X-ray differences between different source types can be correlated with intrinsic source power and with indicators of the viewing angle.

## 7. SUMMARY AND SOME KEY EXPERIMENTS

Jets occur often, in a wide range of extragalactic sources, and with properties well correlated with those of the compact radio cores; thus, it is reasonable to relate them to the fundamental process of energy transport from the cores to the lobes. Their presence supports continuous flow source models and shows that collimation, particle acceleration, and magnetic field amplification probably all occur on both parsec and kiloparsec scales in extragalactic sources. Beyond this, knowledge of jet physics is fragmentary, mainly because we lack credible estimates of jet densities and have only loose, model-dependent constraints on their velocities. Some important questions may be answerable, however, by observations with present or planned instruments:

1. How well does sidedness on parsec and kiloparsec scales correlate with core superluminal motion? Does superluminal motion occur in the cores of sources that should be oriented toward the plane of the sky (e.g. very large lobe-dominated sources)? (Both require sensitive, high dynamic range phase-closure VLBI mapping of cores that are not selected for high flux density alone.)
2. How asymmetric are one-sided kiloparsec-scale jets? Mild brightness

asymmetries $\mathcal{S}$, compatible with weak Doppler boosting (Section 6.1.7) or small differences in the ratio of radiative losses to bulk energy flux, are much easier to explain in large samples than $\mathcal{S} \geq 100:1$ (Sections 6.1.7 and 6.5). (This requires high dynamic range maps of large jets whose cores are not too dominant.)

3. Are jets brighter relative to the lobes when the core is also brighter? Does the answer vary with FR class or optical identification? (This requires unbiased statistics of core, jet, and lobe powers for identified sources.)
4. Can studies of the lobes distinguish the Doppler boosting, asymmetric dissipation, or "flip-flop" models of jet sidedness (Sections 6.2 and 6.3)? (This requires studies of the shapes, spectra, and degrees of polarization of hot spots in jetted and unjetted lobes.)
5. Are jets confined thermally or magnetically (Section 4.1)? Thermal confinement can be tested by high-resolution X-ray imaging and temperature determinations of the environs of recollimating jets, and magnetic confinement may be checked by radio polarimetry of jet cocoons (Section 4.1.3).
6. Can sharp brightness gradients in knots in kiloparsec-scale jets be used to constrain models for jet one sidedness (80)? (This requires proper-motion studies of knots in nearby kiloparsec-scale jets.)
7. Do any jets unambiguously show depolarization that cannot be attributed to foreground Faraday screens, and that might therefore be used to indicate jet densities (Section 6.1)?

Finally, radio, optical, or X-ray spectroscopic evidence for outflow in jets will be welcome now that jets are being interpreted as tracers of the paths of energy transfer in all extragalactic sources.

## Acknowledgments

We are indebted to many colleagues who sent us unpublished data on jets, and who are credited individually in the footnotes to Table 1. We also thank Robert Laing, Bob Sanders, and Dick Henriksen for many invigorating discussions, and Peter Scheuer for valuable criticism of an early draft of this review.

*Literature Cited*

1. Arp, H. C. 1967. *Astrophys. Lett.* 1:1
2. Arp, H. C. 1981. *Proc. ESO/ESA Workshop, 2nd, Optical Jets in Galaxies*, ed. B. Battrick, J. Mort, p. 53. *ESA SP-162*
3. Baade, W., Minkowski, R. 1954. *Ap. J.* 119:215
4. Baan, W. A. 1980. *Ap. J.* 239:433
5. Baldwin, J. A., Carswell, R. F., Wampler, E. J., Smith, H. E., Burbidge, E. M., Boksenberg, A. 1980. *Ap. J.* 236:388
6. Balick, B., Heckman, T. M., Crane, P. C. 1982. *Ap. J.* 254:483

7. Bartel, N. 1984. *Proc. IAU Symp. 110, VLBI and Compact Radio Sources*, ed. G. Setti, K. I. Kellermann. Dordrecht: Reidel. In press
8. Begelman, M. C. 1982. See Ref. 117, p. 223
9. Begelman, M. C., Blandford, R. D., Rees, M. J. 1980. *Nature* 287:307
10. Begelman, M. C., Rees, M. J., Blandford, R. D. 1979. *Nature* 279:770
11. Benford, G. 1979. *MNRAS* 183:29
12. Benford, G. 1981. *Ap. J.* 247:792
13. Benford, G. 1982. See Ref. 117, p. 231
14. Benford, G. 1983. See Ref. 92a, p. 271
15. Benford, G., Ferrari, A., Trussoni, E. 1980. *Ap. J.* 241:98
16. Bicknell, G. V., Henriksen, R. N. 1980. *Astrophys. Lett.* 21:29
17. Bicknell, G. V., Melrose, D. 1983. *Ap. J.* 262:511
18. Biretta, J. A., Owen, F. N., Hardee, P. E. 1983. *Ap. J. Lett.* 274:L27
19. Birkinshaw, M., Laing, R. A., Peacock, J. A. 1981. *MNRAS* 197:253
20. Blanco, V. M., Graham, J. A., Lasker, B. M., Osmer, P. S. 1975. *Ap. J. Lett.* 198:L63
21. Blandford, R. D. 1983. *Astron. J.* 88:245
22. Blandford, R. D., Icke, V. 1978. *MNRAS* 185:527
23. Blandford, R. D., Königl, A. 1979. *Ap. J.* 232:34
24. Blandford, R. D., Königl, A. 1982. *Astrophys. Lett.* 20:15
25. Blandford, R. D., Rees, M. J. 1974. *MNRAS* 169:395
26. Booler, R. V., Pedlar, A., Davies, R. D. 1982. *MNRAS* 199:229
27. Bridle, A. H. 1982. See Ref. 117, p. 121
28. Bridle, A. H., Chan, K. L., Henriksen, R. N. 1981. *J. R. Astron. Soc. Can.* 75:69
29. Bridle, A. H., Davis, M. M., Fomalont, E. B., Willis, A. G., Strom, R. G. 1979. *Ap. J. Lett.* 228:L9
30. Bridle, A. H., Davis, M. M., Meloy, D. A., Fomalont, E. B., Strom, R. G., Willis, A. G. 1976. *Nature* 262:179
31. Bridle, A. H., Fomalont, E. B., Palimaka, J. J., Willis, A. G. 1981. *Ap. J.* 248:499
32. Bridle, A. H., Henriksen, R. N., Chan, K. L., Fomalont, E. B., Willis, A. G., Perley, R. A. 1980. *Ap. J. Lett.* 241:L145
33. Bridle, A. H., Perley, R. A. 1983. See Ref. 92a, p. 57
34. Brodie, J., Königl, A., Bowyer, S. 1983. See Ref. 92a, p. 145
35. Brown, R. L. 1982. *Ap. J.* 262:110
36. Brown, R. L., Johnston, K. J., Lo, K. Y. 1981. *Ap. J.* 250:155
37. Browne, I. W. A. 1983. *MNRAS* 204:23p
38. Browne, I. W. A., Clark, R. R., Moore, P. K., Muxlow, T. W. B., Wilkinson, P. N., et al. 1982. *Nature* 299:788
39. Browne, I. W. A., Orr, M. J. L. 1981. *Proc. ESO/ESA Workshop, 2nd, Optical Jets in Galaxies*, ed. B. Battrick, J. Mort, p. 87. *ESA SP-162*
40. Burbidge, E. M., Smith, H. E., Burbidge, G. R. 1975. *Ap. J. Lett.* 199:L137
41. Burbidge, E. M., Smith, H. E., Burbidge, G. R. 1978. *Ap. J.* 219:400
42. Burch, S. F. 1979. *MNRAS* 187:187
43. Burns, J. O. 1981. *MNRAS* 195:523
44. Burns, J. O. 1983. See Ref. 92a, p. 67
45. Burns, J. O., Balonek, T. 1982. *Ap. J.* 263:546
46. Burns, J. O., Christiansen, W. A. 1980. *Nature* 287:208
47. Burns, J. O., Christiansen, W. A., Hough, D. H. 1982. *Ap. J.* 257:538
48. Burns, J. O., Feigelson, E. D., Schreier, E. J. 1983. *Ap. J.* 273:128
49. Burns, J. O., Gregory, S. A. 1982. *Astron. J.* 87:1245
50. Burns, J. O., Owen, F. N. 1980. *Astron. J.* 85:204
51. Burns, J. O., Schwendeman, E., White, R. A. 1983. *Ap. J.* 271:575
52. Butcher, H. R., van Breugel, W. J. M., Miley, G. K. 1980. *Ap. J.* 235:749
53. Chan, K. L., Henriksen, R. N. 1980. *Ap. J.* 241:534
54. Charlesworth, M., Spencer, R. E. 1982. *MNRAS* 200:933
55. Cohen, M. 1982. *Publ. Astron. Soc. Pac.* 94:266
56. Cohen, M. H., Readhead, A. C. S. 1979. *Ap. J. Lett.* 233:L101
57. Cohen, M. H., Unwin, S. C. 1982. See Ref. 117, p. 345
58. Cohen, M. H., Unwin, S. C., Lind, K. R., Moffet, A. T., Simon, R. S., et al. 1983. *Ap. J.* 272:383
59. Cohen, M. H., Unwin, S. C., Pearson, T. J., Seielstad, G. A., Simon, R. S., et al. 1983. *Ap. J. Lett.* 269:L1
60. Cohen, M. H., Unwin, S. C., Simon, R. S., Seielstad, G. A., Pearson, T. J., et al. 1981. *Ap. J.* 247:774
61. Cohn, H. 1983. *Ap. J.* 269:500
62. Condon, J. J., Condon, M. A., Gisler, G., Puschell, J. J. 1982. *Ap. J.* 252:102
63. Condon, J. J., Mitchell, K. J. 1984. *Ap. J.* 276:472
64. Conway, R. G. 1982. See Ref. 117, p. 167
65. Cornwell, T. J., Perley, R. A. 1982. See Ref. 117, p. 139
66. Cornwell, T. J., Wilkinson, P. N. 1981. *MNRAS* 196:1067
67. Cotton, W. D., Shapiro, I. I., Wittels, J. J. 1981. *Ap. J. Lett.* 244:L57

68. Davies, J. G., Anderson, B., Morison, I. 1980. *Nature* 288:64
69. Davis, R. J., Stannard, D., Conway, R. G. 1978. *MNRAS* 185:435
70. De Pater, I., Perley, R. A. 1983. *Ap. J.* 273:64
71. de Vaucouleurs, G., Nieto, J.-L. 1979. *Ap. J.* 231:364
72. De Young, D. S. 1980. *Ap. J.* 241:81
73. De Young, D. S. 1981. *Nature* 293:43
74. De Young, D. S. 1982. See Ref. 117, p. 69
75. Dreher, J. W. 1982. See Ref. 117, p. 135
76. Drury, L. O. 1983. *Rep. Prog. Phys.* 46: 973
77. Dufour, R. J., van den Bergh, S. 1978. *Ap. J. Lett.* 226:L73
78. Eichler, D. 1982. *Ap. J.* 263:571
79. Eichler, D. 1983. *Ap. J.* 272:48
80. Eichler, D., Smith, M. 1983. *Nature* 303:779
81. Eilek, J. A., Burns, J. O., O'Dea, C. P., Owen, F. N. 1984. *Ap. J.* 278:37
82. Eilek, J. A., Henriksen, R. N. 1982. See Ref. 117, p. 233
83. Ekers, R. D., Fanti, R., Lari, C., Parma, P. 1981. *Astron. Astrophys.* 101:194
84. Ekers, R. D., van Gorkom, J. H., Schwarz, U. J., Goss, W. M. 1983. *Astron. Astrophys.* 122:143
85. Fabricant, D., Lecar, M., Gorenstein, P. 1980. *Ap. J.* 241:552
86. Fanaroff, B. L., Riley, J. M. 1974. *MNRAS* 167:31p
87. Fanti, R. 1983. See Ref. 92a, p. 253
88. Fanti, R., Lari, C., Parma, P., Bridle, A. H., Ekers, R. D., Fomalont, E. B. 1982. *Astron. Astrophys.* 110:169
89. Fanti, R., Padrielli, L., Salvati, M. 1982. See Ref. 117, p. 317
90. Feigelson, E. D. 1983. See Ref. 92a, p. 165
91. Feigelson, E. D., Schreier, E. J., Delvaille, J. P., Giacconi, R., Grindlay, J. E., Lightman, A. P. 1981. *Ap. J.* 251: 31
92. Ferrari, A., Massaglia, S., Trussoni, E. 1982. *MNRAS* 198:1065

92a. Ferrari, A., Pacholczyk, A. G., eds. 1983. *Proc. Int. Workshop Astrophys. Jets.* Dordrecht: Reidel. 327 pp.

93. Ferrari, A., Trussoni, E., Zaninetti, L. 1978. *Astron. Astrophys.* 64:43
94. Ferrari, A., Trussoni, E., Zaninetti, L. 1979. *Astron. Astrophys.* 79:190
95. Ferrari, A., Trussoni, E., Zaninetti, L. 1981. *MNRAS* 196:1051
96. Fomalont, E. B. 1981. *Proc. IAU Symp. 94, Origin of Cosmic Rays*, ed. G. Setti, G. Spada, A. W. Wolfendale, p. 111. Dordrecht: Reidel
97. Fomalont, E. B. See Ref. 92a, p. 37
98. Fomalont, E. B., Bridle, A. H., Miley, G. K. 1982. See Ref. 117, p. 173
99. Fomalont, E. B., Bridle, A. H., Willis, A. G., Perley, R. A. 1980. *Ap. J.* 237:418
100. Fomalont, E. B. Palimaka, J. J., Bridle, A. H. 1980. *Astron. J.* 85:981
101. Fort, D. N., Yee, H. K. C. 1976. *Astron. Astrophys.* 50:19
102. Ghigo, F. D., Rudnick, L., Johnston, K. J., Wehinger, P. A., Wyckoff, S. 1982. See Ref. 117, p. 43
103. Goss, W. M., Wellington, K. J., Christiansen, W. N., Lockhart, I. A., Watkinson, A., et al. 1977. *MNRAS* 178:525
104. Gower, A. C., Gregory, P. C., Hutchings, J. B., Unruh, W. G. 1982. *Ap. J.* 262:478
105. Gower, A. C., Hutchings, J. B. 1982. *Ap. J. Lett.* 258:L63
106. Graham, J. A. 1983. *Ap. J.* 269:440
107. Graham, J. A., Price, R. M. 1981. *Ap. J.* 247:813
108. Greenfield, P. E., Burke, B. F., Roberts, D. H. 1980. *Nature* 286:865
109. Greenfield, P. E., Roberts, D. H., Burke, B. F. 1980. *Science* 208:495
110. Hardee, P. E. 1979. *Ap. J.* 234:47
111. Hardee, P. E. 1982. *Ap. J.* 257:509
112. Hardee, P. E. 1983. *Ap. J.* 269:94
113. Hargrave, P. J., Ryle, M. 1974. *MNRAS* 166:305
114. Hazard, C., Mackey, M. B., Shimmins, A. J. 1963. *Nature* 197:1037
115. Heckman, T. M. 1983. *Ap. J. Lett.* 271: L5
116. Heckman, T. M., Miley, G. K., Balick, B., van Breugel, W. J. M., Butcher, H. R. 1982. *Ap. J.* 262:529
117. Heeschen, D. S., Wade, C. M., eds. 1982. *Proc. IAU Symp. 97, Extragalactic Radio Sources.* Dordrecht: Reidel. 490 pp.
118. Henriksen, R. N., Bridle, A. H., Chan, K. L. 1982. *Ap. J.* 257:63
119. Henriksen, R. N., Vallée, J. P., Bridle, A. H. 1981. *Ap. J.* 249:40
120. Hjellming, R. M., Johnston, K. J. 1982. See Ref. 117, p. 197
121. Hummel, E., Kotanyi, C. G., van Gorkom, J. H. 1983. *Ap. J. Lett.* 267:L5
122. Hunstead, R. W., Murdoch, H. S., Condon, J. J., Phillips, M. M. 1984. *MNRAS* 207:55
123. Icke, V. 1981. *Ap. J. Lett.* 246:L65
124. Icke, V. 1983. *Ap. J.* 265:648
125. Jenkins, C. R. 1982. *MNRAS* 200:705
126. Jones, D. L., Sramek, R. A., Terzian, Y. 1981. *Ap. J.* 246:28
127. Jones, D. L., Sramek, R. A., Terzian, Y. 1981. *Ap. J. Lett.* 247:L57
128. Jones, T., Owen, F. N. 1979. *Ap. J.* 234:818
129. Kahn, F. D. 1983. *MNRAS* 202:553
130. Kapahi, V. K., Saikia, D. J. 1982. *J. Astrophys. Astron.* 3:465

131. Kellermann, K. I. 1983. In *Highlights of Astronomy*, ed. R. M. West, 6:481. Dordrecht: Reidel
132. Kellermann, K. I., Downes, A. J. B., Pauliny-Toth, I. I. K., Preuss, E., Shaffer, D. B., Witzel, A. 1981. *Astron. Astrophys.* 97:L1
133. Königl, A. 1982. *Ap. J.* 261:115
134. Kotanyi, C. G., Ekers, R. D. 1979. *Astron. Astrophys.* 73:L1
135. Laing, R. A. 1980. *MNRAS* 193:427
136. Laing, R. A. 1980. *MNRAS* 193:439
137. Laing, R. A. 1981. *Ap. J.* 248:87
138. Laing, R. A. 1982. See Ref. 117, p. 161
139. Laing, R. A. 1983. In *Highlights of Astronomy*, ed. R. M. West, 6:731. Dordrecht: Reidel
140. Laing, R. A., Riley, J. M., Longair, M. S. 1983. *MNRAS* 204:151
141. Lelièvre, G., Nieto, J.-L., Horville, D., Renard, L., Servan, B. 1984. *Astron. Astrophys.* In press
142. Linfield, R. 1981. *Ap. J.* 244:436
143. Linfield, R. 1981. *Ap. J.* 250:464
144. Linfield, R. 1982. *Ap. J.* 254:465
145. Linfield, R., Perley, R. A. 1984. *Ap. J.* In press
146. Longair, M. S., Riley, J. M. 1979. *MNRAS* 186:625
147. Longair, M. S., Ryle, M., Scheuer, P. A. G. 1973. *MNRAS* 164:243
148. Lonsdale, C. J., Hartley-Davies, R., Morison, I. 1983. *MNRAS* 202:1p
149. Lonsdale, C. J., Morison, I. 1983. *MNRAS* 203:833
150. Lorre, J. J., Nieto, J.-L. 1984. *Astron. Astrophys.* 130:167
151. Lupton, R. H., Gott, J. R. 1982. *Ap. J.* 255:408
152. Maccagni, D., Tarenghi, M. 1981. *Ap. J.* 243:42
153. Machalski, J., Condon, J. J. 1983. *Astron. J.* 88:143
154. Margon, B. 1981. *Ann. NY Acad. Sci.* 375:403
155. Marscher, A. P., Broderick, J. J. 1981. *Ap. J. Lett.* 247:L49
156. Masson, C. R. 1979. *MNRAS* 187:253
157. Miley, G. K. 1980. *Ann. Rev. Astron. Astrophys.* 18:165
158. Miley, G. K. 1983. See Ref. 92a, p. 99
159. Miley, G. K., Heckman, T. M., Butcher, H. R., van Breugel, W. J. M. 1981. *Ap. J. Lett.* 247:L5
160. Miley, G. K., Hogg, D. E., Basart, J. 1970. *Ap. J. Lett.* 159:L19
161. Miley, G. K., Wellington, K. J., van der Laan, H. 1975. *Astron. Astrophys.* 38:381
162. Morrison, P. 1969. *Ap. J.* 157:L73
163. Neff, S. G. 1982. See Ref. 117, p. 137
164. Nieto, J.-L. 1983. See Ref. 92a, p. 113
165. Nieto, J.-L., Lelièvre, G. 1982. *Astron. Astrophys.* 109:95
166. Norman, M. L., Smarr, L., Winkler, K.-H. A., Smith, M. D. 1982. *Astron. Astrophys.* 113:285
167. Norman, M. L., Winkler, K.-H. A., Smarr, L. 1983. See Ref. 92a, p. 227
168. Northover, K. J. E. 1973. *MNRAS* 165:369
169. Orr, M. J. L., Browne, I. W. A. 1982. *MNRAS* 200:1067
170. Osmer, P. S. 1978. *Ap. J. Lett.* 226:L79
171. Owen, F. N., Burns, J. O., Rudnick, L. 1978. *Ap. J. Lett.* 226:L119
172. Owen, F. N., Hardee, P. E., Bignell, R. C. 1980. *Ap. J. Lett.* 239:L11
173. Owen, F. N., Puschell, J. J. 1984. *Astron. J.* In press
174. Parma, P. 1982. See Ref. 117, p. 193
175. Pauliny-Toth, I. I. K., Preuss, E., Witzel, A., Graham, D., Kellermann, K. I., Rönnäng, B. 1981. *Astron. J.* 86:371
176. Pearson, T. J., Readhead, A. C. S. 1981. *Ap. J.* 248:61
177. Pearson, T. J., Readhead, A. C. S., Wilkinson, P. N. 1980. *Ap. J.* 236:714
178. Pearson, T. J., Unwin, S., Cohen, M. H., Linfield, R., Readhead, A. C. S., et al. 1981. *Nature* 290:365
179. Pedlar, A., Booler, R. V., Davies, R. D. 1983. *MNRAS* 203:667
180. Pedlar, A., Booler, R. V., Spencer, R. E., Stewart, O. J. 1983. *MNRAS* 202:647
181. Perley, R. A. 1981. *Proc. ESO/ESA Workshop, 2nd, Optical Jets in Galaxies*, ed. B. Battrick, J. Mort, p. 77. *ESA SP-162*
182. Perley, R. A. 1982. See Ref. 117, p. 175
183. Perley, R. A., Bridle, A. H., Willis, A. G. 1984. *Ap. J. Suppl.* 54:291
184. Perley, R. A., Bridle, A. H., Willis, A. G., Fomalont, E. B. 1980. *Astron. J.* 85:499
185. Perley, R. A., Fomalont, E. B., Johnston, K. J. 1982. *Ap. J. Lett.* 255:L93
186. Perley, R. A., Willis, A. G., Scott, J. S. 1979. *Nature* 281:437
187. Peterson, B. A., Dickens, R. J., Cannon, R. D. 1975. *Proc. Astron. Soc. Aust.* 2:366
188. Phillips, M. M. 1981. *MNRAS* 197:659
189. Porcas, R. W., Booth, R. S., Browne, I. W. A., Walsh, D., Wilkinson, P. N. 1981. *Nature* 289:758
190. Potash, R. I., Wardle, J. F. C. 1979. *Astron. J.* 84:707
191. Potash, R. I., Wardle, J. F. C. 1980. *Ap. J.* 239:42
192. Preston, R. A., Wehrle, A. E., Morabito, D. D., Jauncey, D. L., Batty, M. J., et al. 1983. *Ap. J. Lett.* 266:L93
193. Preuss, E., Alef, A., Pauliny-Toth, I. I. K., Kellermann, K. I. 1982. See Ref. 117, p. 289

194. Preuss, E., Alef, W., Whyborn, A., Wilkinson, P. N., Kellermann, K. I. 1984. *Proc. IAU Symp. 110, VLBI and Compact Radio Sources*, ed. G. Setti, K. I. Kellermann. Dordrecht: Reidel. In press
195. Ray, T. P. 1981. *MNRAS* 196:195
196. Ray, T. P. 1982. *MNRAS* 198:617
197. Readhead, A. C. S. 1980. *Proc. IAU Symp. 92, Objects of High Redshift*, ed. G. O. Abell, P. J. E. Peebles, p. 165. Dordrecht: Reidel
198. Readhead, A. C. S., Cohen, M. H., Blandford, R. D. 1978. *Nature* 272:131
199. Readhead, A. C. S., Cohen, M. H., Pearson, T. J., Wilkinson, P. N. 1978. *Nature* 276:768
200. Readhead, A. C. S., Hough, D. H., Ewing, M. S., Walker, R. C., Romney, J. 1983. *Ap. J.* 265:107
201. Readhead, A. C. S., Napier, P. J., Bignell, R. C. 1980. *Ap. J. Lett.* 237: L55
202. Readhead, A. C. S., Wilkinson, P. N. 1978. *Ap. J.* 223:25
203. Readhead, A. C. S., Wilkinson, P. N. 1980. *Ap. J.* 235:11
204. Rees, M. J. 1971. *Nature* 229:312
205. Rees, M. J. 1978. *Nature* 275:516
206. Rees, M. J. 1978. *MNRAS* 184:61p
207. Rees, M. J. 1982. See Ref. 117, p. 211
208. Rees, M. J., Begelman, M. C., Blandford, R. D. 1981. *Proc. Texas Symp., 10th, Ann. NY Acad. Sci.* 315:254
209. Reid, M. J., Schmitt, J. H. M. M., Owen, F. N., Booth, R. S., Wilkinson, P. N., et al. 1982. *Ap. J.* 263:615
210. Riley, J. M., Pooley, G. G. 1975. *Mem. R. Astron. Soc.* 80:105
211. Robertson, J. G. 1980. *Nature* 286:579
212. Robson, D. W. 1981. *Nature* 294:57
213. Rudnick, L. 1982. See Ref. 117, p. 47
214. Rudnick, L., Burns, J. O. 1981. *Ap. J. Lett.* 246:L69
215. Saikia, D. J. 1981. *MNRAS* 197:11p
216. Saikia, D. J., Cornwell, T. J. 1983. See Ref. 92a, p. 53
217. Saikia, D. J., Shastri, P., Cornwell, T. J., Banhatti, D. G. 1983. *MNRAS* 203: 53p
218. Saikia, D. J., Wiita, P. J. 1982. *MNRAS* 200:83
219. Sanders, R. H. 1983. *Ap. J.* 266:73
220. Saunders, R., Baldwin, J. E., Pooley, G. G., Warner, P. J. 1982. *MNRAS* 197: 287
221. Scheuer, P. A. G. 1974. *MNRAS* 166: 513
222. Scheuer, P. A. G. 1983. In *Highlights of Astronomy*, ed. R. M. West, 6:735. Dordrecht: Reidel
223. Scheuer, P. A. G., Readhead, A. C. S. 1979. *Nature* 277:182
224. Schilizzi, R. T., de Bruyn, A. G. 1983. *Nature* 303:26
225. Schilizzi, R. T., Miley, G. K., Janssen, F. L. J., Wilkinson, P. N., Cornwell, T. J., Fomalont, E. B. 1981. *Proc. ESO/ESA Workshop, 2nd, Optical Jets in Galaxies*, ed. B. Battrick, J. Mort, p. 97. *ESA SP-162*
226. Schmidt, G. D., Peterson, B. A., Beaver, E. A. 1978. *Ap. J. Lett.* 220:L31
227. Schmidt, M. 1963. *Nature* 197:1040
228. Schreier, E. J., Burns, J. O., Feigelson, E. D. 1981. *Ap. J.* 251:523
229. Schreier, E. J., Feigelson, E. D., Delvaille, J., Giacconi, R., Grindlay, J., et al. 1979. *Ap. J. Lett.* 234:L39
230. Schreier, E. J., Gorenstein, P., Feigelson, E. D. 1982. *Ap. J.* 261:42
231. Schwab, F. R. 1980. *Int. Opt. Comput. Conf., SPIE Vol. 231*, p. 18
232. Schwartz, R. D. 1983. *Ann. Rev. Astron. Astrophys.* 21:209
233. Simon, R. S., Readhead, A. C. S., Moffet, A. T., Wilkinson, P. N., Allen, B., Burke, B. F. 1983. *Nature* 302:487
234. Simon, R. S., Readhead, A. C. S., Moffet, A. T., Wilkinson, P. N., Anderson, B. 1980. *Ap. J.* 236:707
235. Slee, O. B., Sheridan, K. V., Dulk, G. A., Little, A. G. 1983. *Publ. Astron. Soc. Aust.* 5:247
236. Smith, M. D., Norman, C. A. 1981. *MNRAS* 194:771
237. Smith, R. M., Bicknell, G. V., Hyland, A. R., Jones, T. J. 1983. *Ap. J.* 266:69
238. Spangler, S. R. 1979. *Astron. J.* 84:1470
239. Spangler, S. R. 1979. *Ap. J. Lett.* 232:L7
240. Spangler, S. R., Basart, J. P. 1981. *Ap. J.* 243:1103
241. Spencer, J. H., Johnston, K. J., Pauliny-Toth, I. I. K., Witzel, A. 1981. *Ap. J. Lett.* 251:L61
242. Steiner, J. E. 1981. *Ap. J.* 250:469
243. Stocke, J. T., Christiansen, W. A., Burns, J. O. 1982. See Ref. 117, p. 39
244. Stocke, J. T., Rieke, G. H., Lebofsky, M. J. 1981. *Nature* 294:319
245. Strom, R. G., Fanti, R., Parma, P., Ekers, R. D. 1983. *Astron. Astrophys.* 122:305
246. Strom, R. G., Willis, A. G. 1981. *Proc. ESO/ESA Workshop, 2nd, Optical Jets in Galaxies*, ed. B. Battrick, J. Mort, p. 83. *ESA SP-162*
247. Sulentic, J. W., Arp, H. C., Lorre, J. J. 1979. *Ap. J.* 233:44
248. Swarup, G., Sinha, R. P., Saikia, D. J. 1982. *MNRAS* 201:393
249. Tarenghi, M. 1981. *Proc. ESO/ESA Workshop, 2nd, Optical Jets in Galaxies*, ed. B. Battrick, J. Mort, p. 145. *ESA SP-162*
250. Thompson, A. R., Clark, B. G., Wade,

C. M., Napier, P. J. 1980. *Ap. J. Suppl.* 44:151
251. Thorne, K. S., Blandford, R. D. 1982. See Ref. 117, p. 255
252. Trussoni, E., Ferrari, A., Zaninetti, L. 1983. See Ref. 92a, p. 281
253. Turland, B. D. 1975. *MNRAS* 172:181
254. Ulvestad, J. S., Johnston, K. J., Weiler, K. W. 1983. *Ap. J.* 266:18
255. Unwin, S. C., Cohen, M. H., Pearson, T. J., Seielstad, G. A., Simon, R. S., et al. 1983. *Ap. J.* 271:536
256. Vallée, J. P. 1982. *Astron. J.* 87:486
257. Vallée, J. P., Bridle, A. H., Wilson, A. S. 1981. *Ap. J.* 250:66
258. van Breugel, W. J. M. 1980. *Structure in radio galaxies.* PhD thesis. Univ. Leiden. 219 pp.
259. van Breugel, W. J. M., Balick, B., Heckman, T., Miley, G. K., Helfand, D. 1983. *Astron. J.* 88:40
260. van Breugel, W. J. M., Heckman, T. M. 1982. See Ref. 117, p. 61
261. van Breugel, W. J. M., Heckman, T. M., Bridle, A. H., Butcher, H. R., Strom, R. G., Balick, B. 1983. *Ap. J.* 275:61
262. van Breugel, W. J. M., Miley, G. K. 1977. *Nature* 265:315
263. van Breugel, W. J. M., Willis, A. G. 1981. *Astron. Astrophys.* 96:332
264. van der Hulst, J. M., Hummel, E., Dickey, J. M. 1982. *Ap. J. Lett.* 261: L59
265. van Groningen, E., Miley, G. K., Norman, C. 1980. *Astron. Astrophys.* 90:L7
266. Wade, C. M. 1960. *Observatory* 80:235
267. Waggett, P. C., Warner, P. J., Baldwin, J. E. 1977. *MNRAS* 181:465
268. Walker, R. C., Benson, J. M., Seielstad, G. A., Unwin, S. C. 1984. *Proc. IAU Symp. 110, VLBI and Compact Radio Sources*, ed. G. Setti, K. I. Kellermann. Dordrecht: Reidel. In press
269. Walker, R. C., Seielstad, G. A., Simon, R. S., Unwin, S. C., Cohen, M. H., et al. 1981. *Ap. J.* 257:56
270. Wardle, J. F. C., Kronberg, P. P. 1974. *Ap. J.* 194:249
271. Wardle, J. F. C., Potash, R. I. 1982. See Ref. 117, p. 129
272. Wellington, K. J., Miley, G. K., van der Laan, H. 1973. *Nature* 244:502
273. Wiita, P. J., Siah, M. J. 1981. *Ap. J.* 243:710
274. Wilkinson, P. N. 1982. See Ref. 117, p. 149
275. Wilkinson, P. N., Readhead, A. C. S., Purcell, G. H., Anderson, B. 1977. *Nature* 269:764
276. Willingale, R. 1981. *MNRAS* 194:359
277. Willis, A. G. 1981. *Proc. ESO/ESA Workshop, 2nd, Optical Jets in Galaxies*, ed. B. Battrick, J. Mort, p. 71. *ESA SP-162*
278. Willis, A. G., Strom, R. G., Bridle, A. H., Fomalont, E. B. 1981. *Astron. Astrophys.* 95:250
279. Willis, A. G., Strom, R. G., Perley, R. A., Bridle, A. H. 1982. See Ref. 117, p. 141
280. Willis, A. G., Wilson, A. S., Strom, R. G. 1978. *Astron. Astrophys.* 66:L1
281. Wills, B. J. 1982. See Ref. 117, p. 373
282. Wilson, A. S. 1983. In *Highlights of Astronomy*, ed. R. M. West, 6:467. Dordrecht: Reidel
283. Wilson, A. S., Ulvestad, J. S. 1982. *Ap. J.* 263:576
284. Wirth, A., Smarr, L., Gallagher, J. S. 1982. *Astron. J.* 87:602
285. Wyckoff, S., Johnston, K., Ghigo, F., Rudnick, L., Wehinger, P., Boksenberg, A. 1983. *Ap. J.* 265:43
286. Zaninetti, L., Trussoni, E. 1983. See Ref. 92a, p. 309